

HSP90 inhibitor, NVP-AUY922, improves myelination *in vitro* and supports the maintenance of myelinated axons in neuropathic mice

Vinita G. Chittoor-Vinod, Hannah Bazick, Adrian G. Todd, Darin Falk, Kathryn H. Morelli, Robert W. Burgess, Thomas C. Foster, and LUCIA NOTTERPEK

ACS Chem. Neurosci., **Just Accepted Manuscript** • DOI: 10.1021/acchemneuro.9b00105 • Publication Date (Web): 24 Apr 2019

Downloaded from <http://pubs.acs.org> on April 25, 2019

Just Accepted

“Just Accepted” manuscripts have been peer-reviewed and accepted for publication. They are posted online prior to technical editing, formatting for publication and author proofing. The American Chemical Society provides “Just Accepted” as a service to the research community to expedite the dissemination of scientific material as soon as possible after acceptance. “Just Accepted” manuscripts appear in full in PDF format accompanied by an HTML abstract. “Just Accepted” manuscripts have been fully peer reviewed, but should not be considered the official version of record. They are citable by the Digital Object Identifier (DOI®). “Just Accepted” is an optional service offered to authors. Therefore, the “Just Accepted” Web site may not include all articles that will be published in the journal. After a manuscript is technically edited and formatted, it will be removed from the “Just Accepted” Web site and published as an ASAP article. Note that technical editing may introduce minor changes to the manuscript text and/or graphics which could affect content, and all legal disclaimers and ethical guidelines that apply to the journal pertain. ACS cannot be held responsible for errors or consequences arising from the use of information contained in these “Just Accepted” manuscripts.



April 17, 2019

HSP90 inhibitor, NVP-AUY922, improves myelination in vitro and supports the maintenance of myelinated axons in neuropathic mice

Vinita G. Chittoor-Vinod¹, Hannah Bazick¹, Adrian G. Todd², Darin Falk², Kathryn H. Morelli^{3,4}, Robert W. Burgess^{3,4}, Thomas C. Foster¹ and Lucia Notterpek^{1,*}

¹Departments of Neuroscience and Neurology, College of Medicine, McKnight Brain Institute, ²Department of Pediatrics, Powell Gene Therapy Center, University of Florida, Gainesville, ³The Graduate School of Biomedical Science and Engineering, University of Maine, Orono, ⁴The Jackson Laboratory, Bar Harbor, Maine

Address for correspondence:

Lucia Notterpek, Ph.D.
Dept. of Neuroscience
1149 Newell Drive, Box 100244,
Gainesville, FL 32610-0244
Phone: 352-294-5374; Fax: 352-392-8347;
Email: notterpek@ufl.edu

Keywords (6) :

Neuropathy; Charcot-Marie-Tooth disease; chaperones; neuromuscular disease; myelin; C22 mice

Chemical Compounds: NVP-AUY922 (PubChem CID: 10096043); BIIB021 (PubChem CID: 16736529); AT13387 (PubChem CID: 11955716); SNX5422 (PubChem CID: 44195571); STA9090 (PubChem CID: 66577018)

Abbreviations used:

PMP22, peripheral myelin protein 22; CMT1A, Charcot-Marie-Tooth disease type 1A; HSP, heat shock protein; Wt, Wild type

1
2
3 **41 ABSTRACT**
4 **42**

5 43 Hereditary demyelinating neuropathies linked to peripheral myelin protein 22 (PMP22) involve
6 44 the disruption of normal protein trafficking and are therefore relevant targets for chaperone
7 45 therapy. Using a small molecule HSP90 inhibitor, EC137, in cell culture models, we previously
8 46 validated the chaperone pathway as a viable target for therapy development. Here, we tested
9 47 five commercially available inhibitors of HSP90 and identified, BIIB021 and AUY922, to support
10 48 Schwann cell viability and enhance chaperone expression. AUY922 showed higher efficacy,
11 49 compared to BIIB021, in enhancing myelin synthesis in dorsal root ganglion explant cultures
12 50 from neuropathic mice. For in vivo testing, we randomly assigned 2-3 month old C22 and 6-
13 51 week old Trembler J (TrJ) mice, to receive two weekly-injections of either vehicle or AUY922 (2
14 52 mg/kg). By the i.p. route, the drug was well-tolerated by all mice over the 5-month long study,
15 53 without influence on body weight or general grooming behavior. AUY922 improved the
16 54 maintenance of myelinated nerves of both neuropathic models, and attenuated the decline in
17 55 rotarod performance and peak muscle force production in C22 mice. These studies highlight the
18 56 significance of proteostasis in neuromuscular function and further validate the HSP90 pathway
19 57 as a therapeutic target for hereditary neuropathies.
20
21
22
23
24
25
26
27
28
29
30
31
32
33
34
35
36
37
38
39
40
41
42
43
44
45
46
47
48
49
50
51
52
53
54
55
56
57

INTRODUCTION

The heat shock (HS) pathway represents a cellular stress response, which results in elevated expression of cytoprotective chaperones, or heat shock proteins (HSPs). Activation of chaperones has been shown to reduce the aggregation of misfolded proteins and alleviate disease phenotypes in various neurodegenerative disease models¹⁻³. It has been proposed that an increase in the availability of functional HSPs aids in the folding, and the disaggregation or enhanced degradation of misfolded proteins⁴⁻⁶. The activation of HS pathway can be achieved through inhibition of HSP90, which disrupts its interaction with Heat Shock Factor-1 (HSF-1) leading to transcriptional activation of the HS response⁷. Although HSP90 inhibitors have been investigated primarily for their anti-cancer properties; when used within a defined concentration range, they can be beneficial in the treatment of protein misfolding disorders⁸.

Charcot-Marie-Tooth (CMTs) diseases comprise a heterogeneous group of progressive hereditary peripheral neuropathies, most often associated with overproduction of peripheral myelin protein 22 (PMP22), an aggregation-prone Schwann cell protein⁹⁻¹⁰. Transgenic C22 mice express additional copies of the wild type (Wt) human PMP22 and reproduce the phenotypic traits of the neuropathies, including demyelination of peripheral nerves, impaired locomotor performance and age-associated disease progression¹¹⁻¹³. Mislocalization and aggregation of mutant PMP22 is a culprit in early-onset, severe neuropathies; modeled by the Trembler J (TrJ) mouse carrying a spontaneous mutation in the *Pmp22* gene¹⁴. In a previous study, we showed that activation of the HS pathway using EC137, a synthetic HSP90 inhibitor, reduced the aggregation of PMP22 and improved myelination in neuron-glia explant cultures from C22 mice¹⁵. In an *in vivo* study of neuropathic TrJ mice, an increase in chaperone expression through intermittent fasting supported maintenance of nerve myelin and locomotor performance¹⁶. In accordance, enhancement of the stress response by life-long calorie restriction was beneficial for peripheral nerve integrity in aged rats^{15, 17}. Recent *in vitro* work further supports the importance of heat shock protein 70 (HSP70) in preventing the aggregation of misfolded PMP22 and aiding in its degradation¹⁸. In related studies, pharmacological activation of HSP70 was shown to reverse sensory deficits in diabetic mice¹⁹, and ameliorate nerve demyelination and motor deficits in an inducible neuropathic mouse model²⁰. Thus, a number of experimental scenarios indicate that chaperones are critical for myelin maintenance and peripheral nerve function.

In this study, we screened five commercially available HSP90 inhibitors and identified NVP-AUY922 (referred to as AUY922 or AUY from here on) as the most effective compound in improving myelination in explant cultures from neuropathic C22 mice. This positive response correlated with robust induction of chaperones in Schwann cells, in a dose- and time-dependent manner. *In vivo* administration of AUY922 preserved myelinated peripheral nerves in both C22 and TrJ models, and attenuated the decline in neuromuscular performance in neuropathic C22 mice.

RESULTS

AUY922 and BIIB021 are Non-toxic Inducers of the Chaperone Pathway in Schwann cells

We tested five commercially available HSP90 inhibitors, including AT13387, AUY922, BIIB021, SNX5422 and STA9090 on the viability of rat Schwann cells using the MTS assay. After 24 h exposure, geldanamycin (GA, 50 nM), a well-known inhibitor of HSP90, significantly decreased cellular viability compared to DMSO (Figure 1A), which is in agreement with previous studies²¹. Among these five tested compounds, lower dosages (50 nM) of AT13387, BIIB021 and STA9090 were well-tolerated by Schwann cells, while the higher dosages (500 nM) significantly decreased cellular viability, compared to DMSO. Surprisingly, neither concentration of AUY922 affected cell viability, while SNX5422 was toxic at both concentrations and therefore excluded from subsequent studies.

Next, we determined the efficiency of these compounds in inducing the chaperone pathway, by measuring HSP70 expression in non-myelinating Schwann cells (Figure 1B)²². After 24 h incubation, AUY922 and BIIB021, each at 100 nM, elicited similar HSP70 transcript levels as GA (50 nM), the positive control. In comparison, incubation of the cells with AT13387 and STA9090 lacked positive effects (Figure 1B). Because AUY922 and BIIB021 elicited minimal Schwann cell toxicity and effectively induced the HS response, we chose these two compounds for further testing.

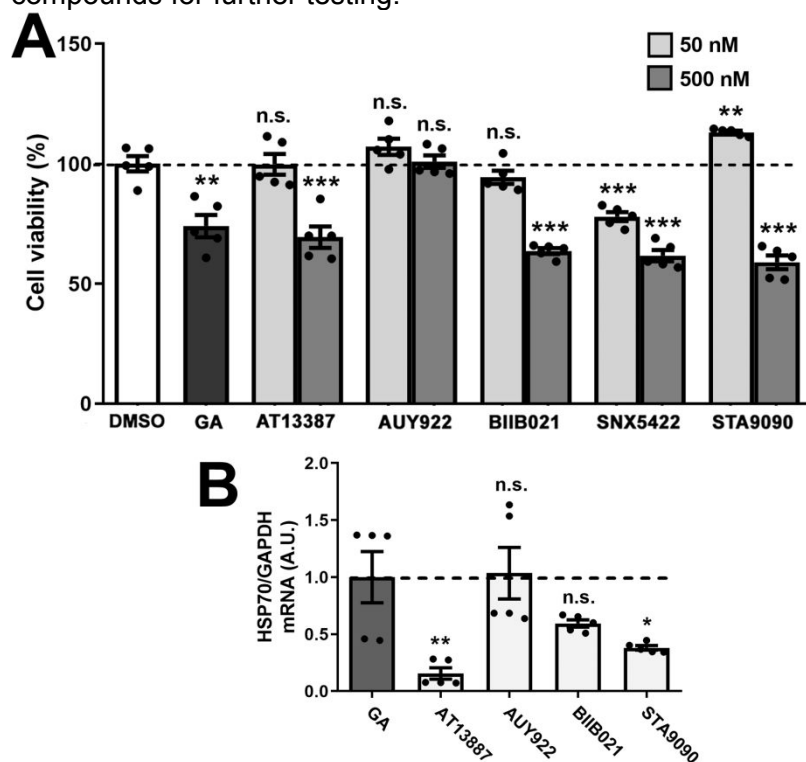
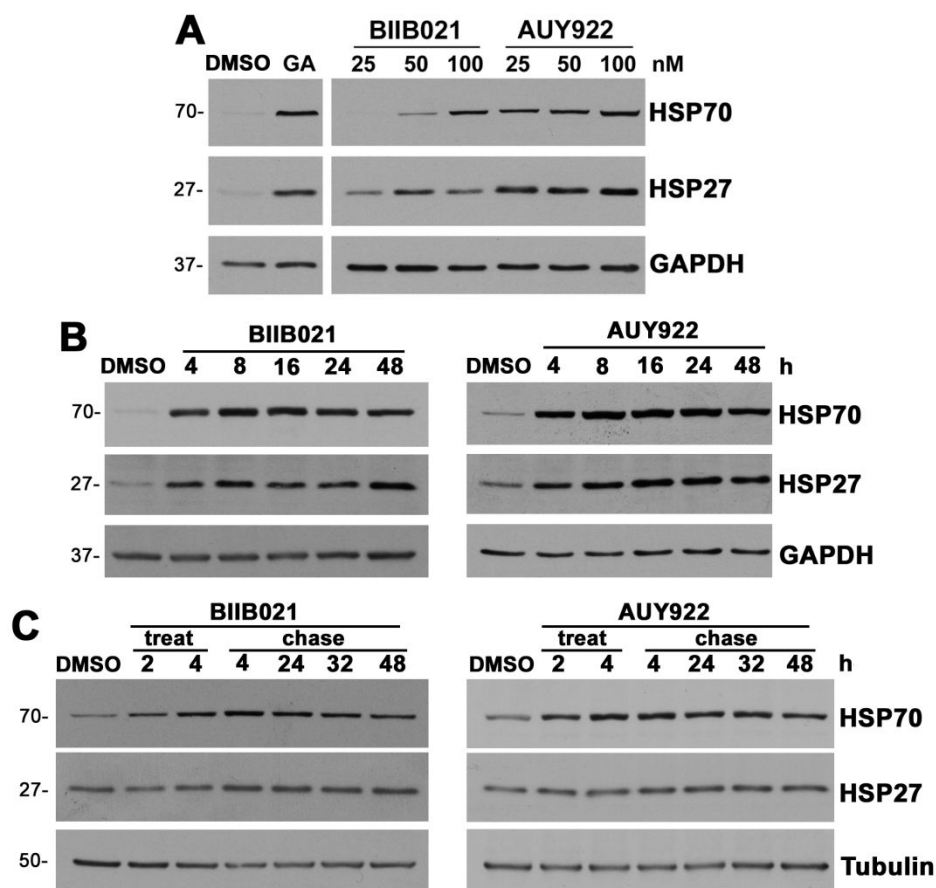


Figure 1. Effects of HSP90 inhibitors on Schwann cells. (A) Cell viability after treatment (24 h) with DMSO, GA (50 nM) or the indicated five HSP90 inhibitors (50 and 500 nM) was calculated and graphed, as percentage of DMSO (vehicle). (B) HSP70 mRNA levels were quantified after 24 h treatment with the indicated compounds (100 nM). GAPDH was used as an internal control. (A, B) GA (50 nM) served as a positive control. A.U.: arbitrary units. Graphs are plotted as means \pm SEM; *** P <0.001; ** P <0.01; * P <0.05; n.s. non-significant; two-tailed Unpaired Student's t -test.

127 To characterize the influence of the two selected compounds on chaperone levels, we
 128 performed dosage and time course studies (Figure 2). First, non-myelinating Schwann cells
 129 were treated with 25, 50 or 100 nM of either BIIB021 or AUY922 for 24 h and then analyzed for
 130 levels of HSP70 and HSP27 (Figure 2A). Both compounds increased HSP70 levels in a dose-
 131 dependent fashion, showing peak expression at 100 nM. Although the levels of HSP27 did not
 132 change prominently with different doses of the test compounds, cells treated with even the
 133 lowest dose showed higher HSP27 expression, as compared to the DMSO controls. However,
 134 AUY922 was more effective in increasing the levels of HSP70 and HSP27, even at lower doses,
 135 as compared to BIIB021. This finding corresponds with the higher levels of HSP70 mRNA
 136 observed upon AUY922 treatment, as compared to BIIB021 (Figure 1B). Next, time course
 137 experiments were performed over 4-48 h incubation periods (Figure 2B). As shown, 100 nM
 138 BIIB021 or AUY922 increased HSP70 levels as early as 4 h, with expression peaking between
 139 16-24 h. To study the sustainability of the induction, Schwann cells were treated with either 100
 140 nM AUY922 or BIIB021 for 4 h (treat), followed by wash out and media replacement without
 141 drugs (chase) (Figure 2C). Cells exposed to BIIB021 or AUY922 for 4 h maintained elevated
 142 chaperone expression for at least 48 h, compared to the DMSO-treated controls. These results
 143 indicate that exposure of Schwann cells to low concentrations of AUY922 or BIIB021 elicits
 144 robust and sustained chaperone induction, without significant cellular toxicity.



145 **Figure 2. Treatment with BIIB021 and AUY922 increase chaperone expression in a dose-**
 146 **and time-dependent manner.** (A) Steady-state levels of HSP70 and HSP27 in whole Schwann
 147 cell lysates (15 μ g/lane) were analyzed after 24 h treatment with DMSO, BIIB021 or AUY922, at
 148 the specified doses. GA (50 nM) served as a positive control. (B) HSP70 and HSP27 levels
 149

1
2
3 150 were observed after treatment with 100 nM BIIB021 or AUY922 for the indicated times. (C)
4 151 Chaperone pathway activation by BIIB021 or AUY922 (100 nM) was studied after 2 or 4 h
5 152 (treatment), followed by 4, 24, 32 and 48 h chase time points. (A, B) GAPDH and (C) tubulin
6 153 served as protein loading controls. Molecular mass on left, in kDa. (A-C) Data shown are
7 154 representative of n=3 independent experiments.
8 155

9 156 **Improved Myelin Production upon Chaperone Induction in Explant Cultures from** 10 157 **Neuropathic Mice** 11 158

12 159 The effects of AUY922 and BIIB021 on the myelination capacity of peripheral glia were
13 160 assessed in dorsal root ganglion (DRG) explant cultures from wild type (Wt) and neuropathic
14 161 C22 mice ¹⁵. DRG explant cultures were treated with either Vehicle (Veh, DMSO), AUY922 (A,
15 162 100 nM) or BIIB021 (B, 100 nM) for 2 weeks, followed by analyses for chaperone expression
16 163 and myelin formation (Figure 3). As shown (Figure 3A), the levels of HSP70 are elevated in
17 164 HSP90 inhibitor-treated (A and B) Wt and C22 cultures, as compared to Vehicle (Veh) controls.
18 165 Within the same protein lysates, myelin production was evaluated through the expression levels
19 166 of myelin protein zero (P0), which constitutes the majority of peripheral myelin proteins (Figure
20 167 3A). Both AUY922 and BIIB021-treated cultures from neuropathic mice show elevated levels of
21 168 P0 compared to the Vehicle control, and this effect was consistent across independent culture
22 169 preparations. To assess the potential contribution of DRG neurons to the increase in
23 170 chaperones, we depleted Wt explants of Schwann cells by anti-mitotic FUdR treatment ¹⁵ (SC
24 171 depleted, Figure 3B). The chaperone response of explant cultures to AUY922 (the more potent
25 172 HSP90 inhibitor) without Schwann cells is muted, indicating that the increase in HSP70
26 173 expression is predominantly from the glial cells.
27 174

28 175 We complemented the biochemical studies on myelin production, with direct evaluation
29 176 of myelin basic protein (MBP) positive internode segments ¹⁵. Measurement and quantification
30 177 of MBP-positive myelin segments in the explant cultures revealed significant increases in
31 178 internode lengths in AUY922-treated Wt and C22 cultures, while the influence of BIIB021 did not
32 179 reach significance in cultures from neuropathic mice (Figure 3C, D). Representative
33 179 micrographs from each treatment paradigm are shown and support the positive impact of the
34 179 two tested compounds on myelin formation (Figure 3E), with AUY922 being more efficacious.
35 180
36
37
38
39
40
41
42
43
44
45
46
47
48
49
50
51
52
53
54
55

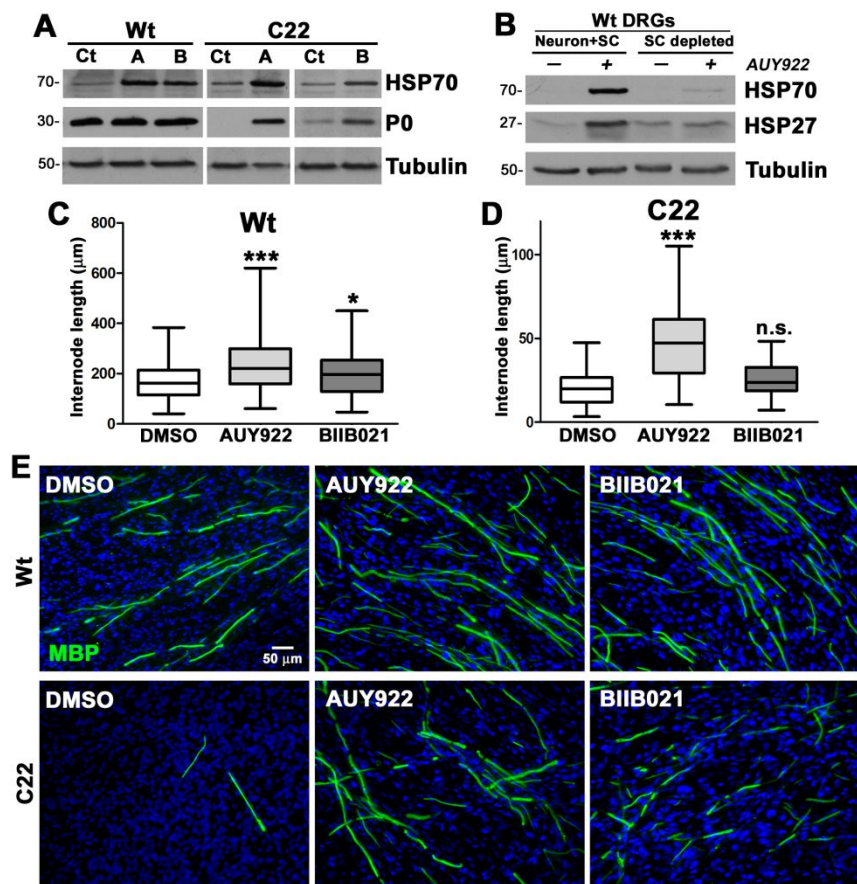


Figure 3. Improved myelin production in DRG explant cultures from C22 mice after treatment with AU922. (A) Steady-state levels of HSP70 and P0 were analyzed in Vehicle (Veh), AU922 or BIIB021 treated explant lysates (35 μg/lane). (B) Wt DRG cultures, with (Neuron + Schwann cell), and without (depleted), Schwann cells were treated with 100 nM AU922 and analyzed for the indicated chaperones. (A, B) Tubulin served as a protein loading control. Molecular mass on left, in kDa. (C, D) MBP-positive myelin internode lengths in explant cultures from Wt (C) and C22 (D) mice treated with Vehicle, AU922 or BIIB021 were measured (n=100-120 segments per group) and graphed as whisker plots with median (center line), quartiles (box), and extremes (whiskers); *** $P < 0.001$; * $P < 0.05$; n.s. non-significant; two-tailed Unpaired Student's t -test. (E) Cultures from Wt (top panel) and C22 (lower panel) mice, treated with the indicated compounds were stained for MBP (green). Nuclei were visualized with Hoechst dye (blue). Scale bar, as shown. Data shown are representative of n=3-4 independent experiments.

AUY922 Supports Neuromuscular Performance in C22 Mice

To test the effects of AU922 on peripheral myelin and motor performance of neuropathic mice, Wt and C22 littermates were randomly segregated at 7 weeks of age into vehicle and AU922 treatment cohorts. Animals were injected via the peritoneum with 2 mg/kg AU922 twice a week, for 20 weeks. Note, this chosen dosing regimen is significantly distinct from the short-term, daily, 50 mg/kg treatment paradigm used for tumor reduction in athymic mice²³. As shown (Figure 4A), the body weight gain of the animals treated with the drug is similar to those injected with vehicle over the period of the study, implying no adverse effects of

1
2
3 205 the drug on the overall health of the mice. Effects of AUY922 treatment on the motor
4 206 performance of Wt and C22 mice were assessed on the accelerating rotarod at the beginning of
5 207 the study, and monthly thereafter. Since biological sex does not affect rotarod performance²⁴⁻²⁵,
6 208 values for male and female mice were combined. At baseline (7 weeks of age), there is a
7 209 significant difference in the ability of Wt and C22 mice to stay on the rotating rod, and this
8 210 difference becomes more pronounced at the end of the study, when the vehicle treated groups
9 211 are compared (Figure 4B, C). This is in agreement with the progressive nature of this disease in
10 212 the C22 model^{13, 26}. At baseline, the vehicle and AUY922 treatment groups of C22 mice do not
11 213 differ in their latencies to fall (Figure 4B), however at the end of the study the AUY922-treated
12 214 C22 mice perform significantly better than vehicle (Figure 4C). An ANOVA on latency for the
13 215 rotating rod was conducted for baseline and for 2, 6, 10, 14, and 20 weeks of treatment (Figure
14 216 4D). Genotype differences were observed for 2, 6, and 10 weeks of treatment. There was a
15 217 tendency ($P = 0.072$) for a genotype difference at week 14, and main effects of genotype
16 218 [$F(1,21) = 9.74$, $P = 0.01$] and treatment [$F(1,21) = 8.49$, $P = 0.01$] were observed for week 20
17 219 (Figure 4D). Post hoc tests indicate that performance of C22 AUY922 mice was not different
18 220 from Wt vehicle treated mice for weeks 14 and 20 (Figure 4C, D). Furthermore, post hoc tests
19 221 examining treatment effects in each genotype indicated that the effect was restricted to C22
20 222 mice. Finally, a repeated measures ANOVA between baseline and week 20 within each
21 223 genotype and treatment group indicated that C22 vehicle treated mice decreased performance
22 224 [$F(1,5) = 7.39$, $P = 0.05$] (Figure 4D).

23 225 Next, to examine the effects of AUY922 on skeletal muscle strength, we performed *in*
24 226 *situ* force-frequency contractile analysis on the tibialis anterior (TA) muscle²⁷⁻²⁹. Absolute
25 227 maximal tetanic force generated by the TA after sequential single stimulations of the common
26 228 peroneal nerve was measured and normalized to the body weight of the animal (Figure 4E). We
27 229 found a significant (~28%) increase in force generation in C22 animals treated with AUY922, as
28 230 compared to vehicle. In addition, assessment of myofiber cross-sectional area within the same
29 231 set of TA muscles revealed a significant improvement, or maintenance, of tissue integrity when
30 232 compared to vehicle (Figure 4F).

31 233 For analyzing the bioavailability of AUY922, blood and liver tissues were collected at the
32 234 end of the study. While all samples were acquired within a 4 h time window of the final injection,
33 235 AUY922 concentration varied in sera and liver; from 2.78 to 226 ng/mL in the sera, and 101 to
34 236 304 ng/g in the liver. Overall, these results indicate that the AUY922 treatment paradigm is well-
35 237 tolerated by neuropathic C22 mice and results in the attenuation of declining neuromuscular
36 238 performance and myofiber atrophy.

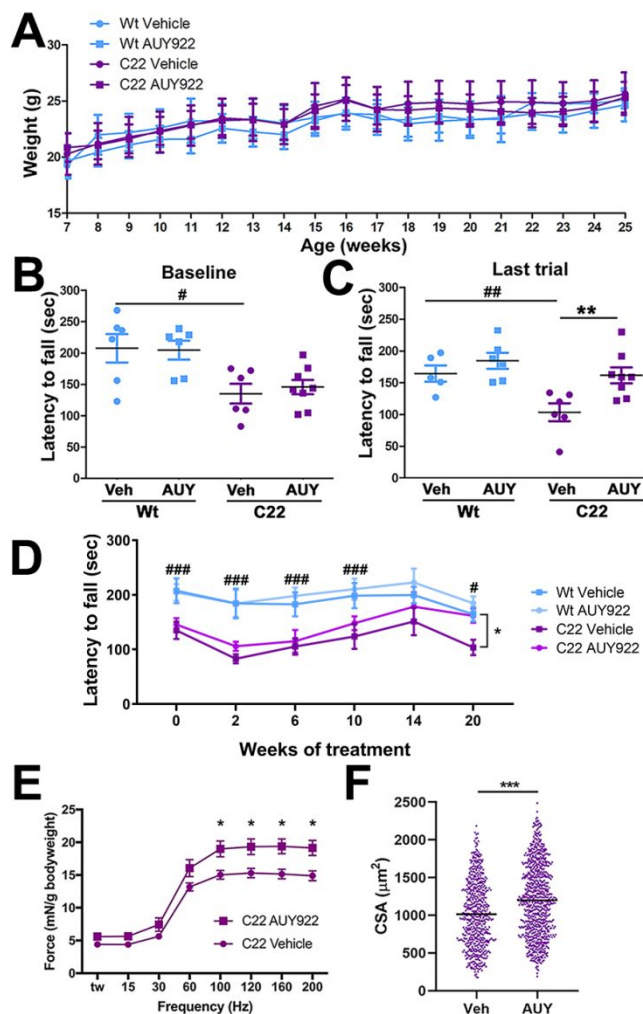


Figure 4. Treatment with AUY922 improves neuromuscular performance of C22 mice. (A) Mean \pm SEM of body weight of Wt and C22 mice ($n=6-8$ mice per group) were plotted over the treatment period. (B-C) Performance of individual animals on the accelerating rotarod at (B) baseline (7 weeks age) and (C) at the end of the treatment (25 weeks age) are shown. The bars represent the mean for each group. (D) Mean \pm SEM of rotarod performance of all groups, plotted over the treatment period. (E) Muscle force, analyzed using an *in situ* technique, was recorded and normalized to the animal's body weight (mN/g= milliNewtons/grams). Each point represents the mean \pm SEM force. (F) Distribution of individual measures of cross-sectional area of TA muscle from C22 mice treated with vehicle or AUY ($n=3-5$ mice per group). The bars represent the mean for each group. For all graphs, # signs indicate a significant ($\#P<0.05$, $##P<0.01$, $###P<0.001$) genotype difference. $*P<0.05$, $**P<0.01$, $***P<0.001$, indicating a significant treatment effect for C22 mice.

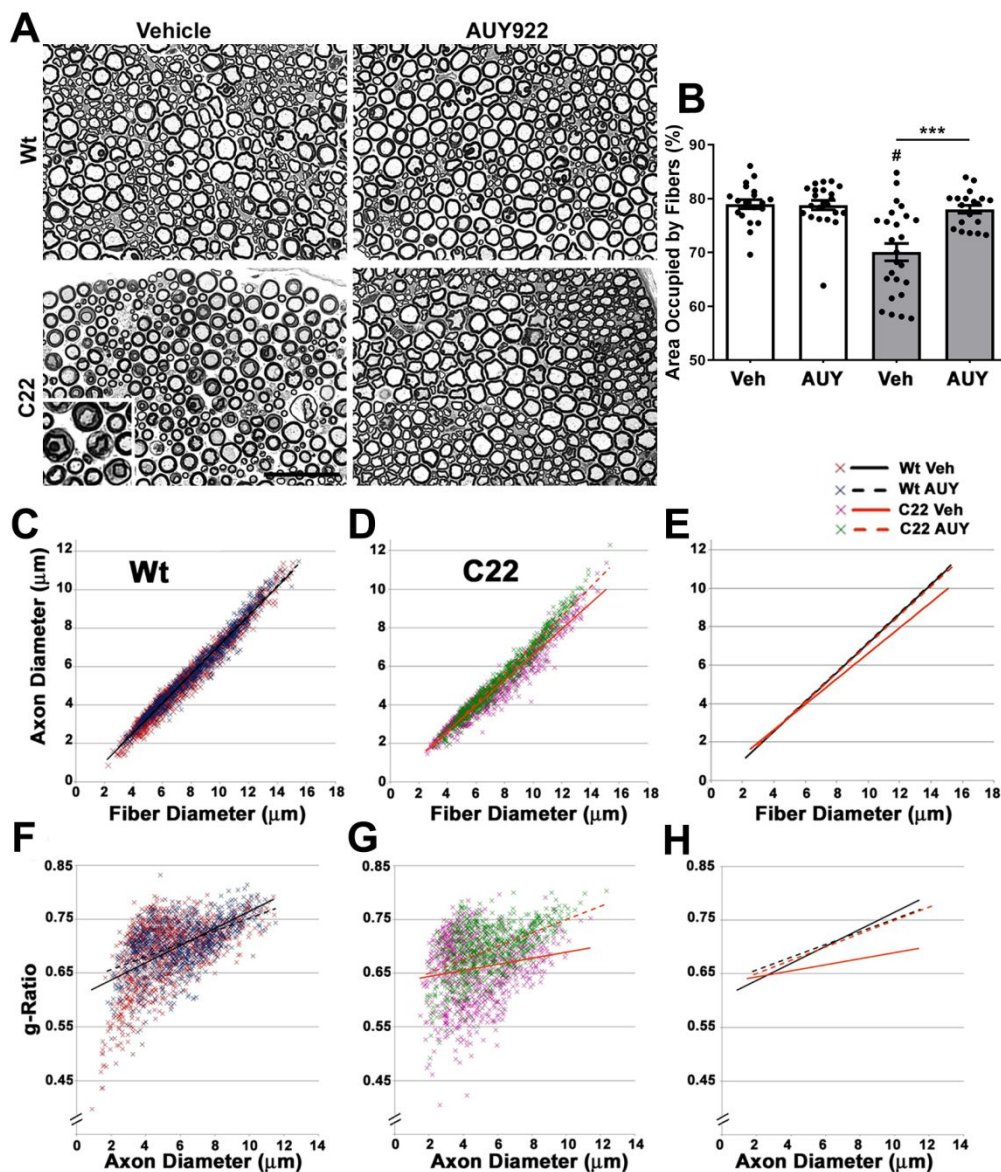
AUY922 Treatment Maintains Myelinated Axons in C22 Neuropathic Mice

Histopathological defects in peripheral nerves of C22 mice include repeated demyelination and remyelination of medium to large axons with onion bulbs, and signs of acute myelin breakdown, with macrophage infiltration^{11; 30}. Cross-sectional analyses of sciatic nerves from the C22 vehicle group revealed these characteristics, when compared to the Wt vehicle

1
2
3 259 group (Figure 5A). However, in our cohort of mice the occurrences of these disease-associated
4 260 pathological features are notably reduced compared with the original publication by the Huxley
5 261 lab ¹¹. Since the severity of C22 phenotype depends on the copy number of the transgene ²⁶,
6 262 we compared archived tissue from ~2007 to tissue from mice used in this study. We found no
7 263 change in transgene copy number by qPCR. We further analyzed the genetic background and
8 264 determined that historically the mice were on a mixed C57BL/6J and C57BL/6N background; but
9 265 owing to our maintenance breeding scheme, they are now on a predominantly CBA
10 266 background. This shift in genetic background likely accounts for changes in severity from
11 267 previous reports. Since all the studies described here use contemporary littermate controls, this
12 268 should not affect the interpretation of the results. Indeed, we found that the nerves from
13 269 AUY922-treated C22 mice contained distinct, well-myelinated axonal profiles, with rare
14 270 occurrence of degenerating fibers and onion bulbs, compared with vehicle (Figure 5A). We
15 271 found no apparent differences in the histology of nerves from Wt mice treated with either vehicle
16 272 or AUY922.

17 273 We corroborated the microscopic observations with morphometric analyses of randomly
18 274 selected cross-sectional nerve areas from independent mice (Figure 5B-H). The total area
19 275 occupied by nerve fibers within a fixed size square is significantly increased in AUY922-treated
20 276 C22 animals, as compared to vehicle (Figure 5B). Upon comparison of axon and fiber
21 277 diameters in Wt groups (Figure 5C-E), we found no deviation in the overall values (co-efficient
22 278 of correlation, $r^2=0.96$ in both vehicle and AUY922 groups). However, in nerves from the C22
23 279 neuropathic animals, we found a delineation between the vehicle ($r^2=0.94$) and AUY922
24 280 ($r^2=0.96$) groups. A similar pattern is obtained when the g-ratios (axon/fiber diameter) were
25 281 analyzed as a function of axon diameter (Figure 6F-H) in nerves of C22 animals ($r^2=0.03$ in
26 282 vehicle versus $r^2=0.23$ in AUY922). This is in contrast to the trend observed in vehicle ($r^2=0.29$)
27 283 and AUY922-treated ($r^2=0.28$) Wt samples. Correlative analysis suggests that an increase in
28 284 fiber diameter in vehicle-injected C22 animals is not accompanied by a proportional increase in
29 285 axon diameter; and this is reflected in the altered g-ratio values. However, this signature is
30 286 rectified with AUY922 treatment where the patterns are comparable to the Wt cohorts. Together,
31 287 these results indicate that bi-weekly injection of AUY922 supports the maintenance of
32 288 myelinated axons in C22 neuropathic mice.

33
34
35
36
37
38
39
40
41
42
43
44
45
46
47
48
49
50
51
52
53
54
55



289
290

291 **Figure 5. AUY922 administration supports the maintenance of myelinated axons in**
 292 **sciatic nerves of C22 mice.** (A) Cross-sectional views of nerve sections from Wt (top panels)
 293 and C22 (lower panels) male mice. Micron bar, 45 μm . (B) Cross-sectional area occupied by
 294 nerve fibers in a 40 μm X 40 μm square (n=20-25 fibers per animal; n=6-8 mice per group) was
 295 measured and graphed as shown. Graph plotted as means \pm SEM; *** P <0.001, across the
 296 treatment groups; # P <0.05, across the genotypes; two-tailed Unpaired Student's t -test. (C-D)
 297 Correlative analyses between axon and fiber diameter measurements were obtained from
 298 sciatic nerve cross-sectional areas from (C) Wt and (D) C22 groups. (E) Comparison of
 299 trendlines between the cohorts in C and D. (F-G) Scatter plots comparing the g-ratios (axon
 300 diameter/fiber diameter) of individual fibers plotted as a function of axon diameters in nerves of
 301 (F) Wt and (G) C22 animals. (C-H) n=950-1100 fibers per group. (H) Trendline comparisons of
 302 graphs in F and G.

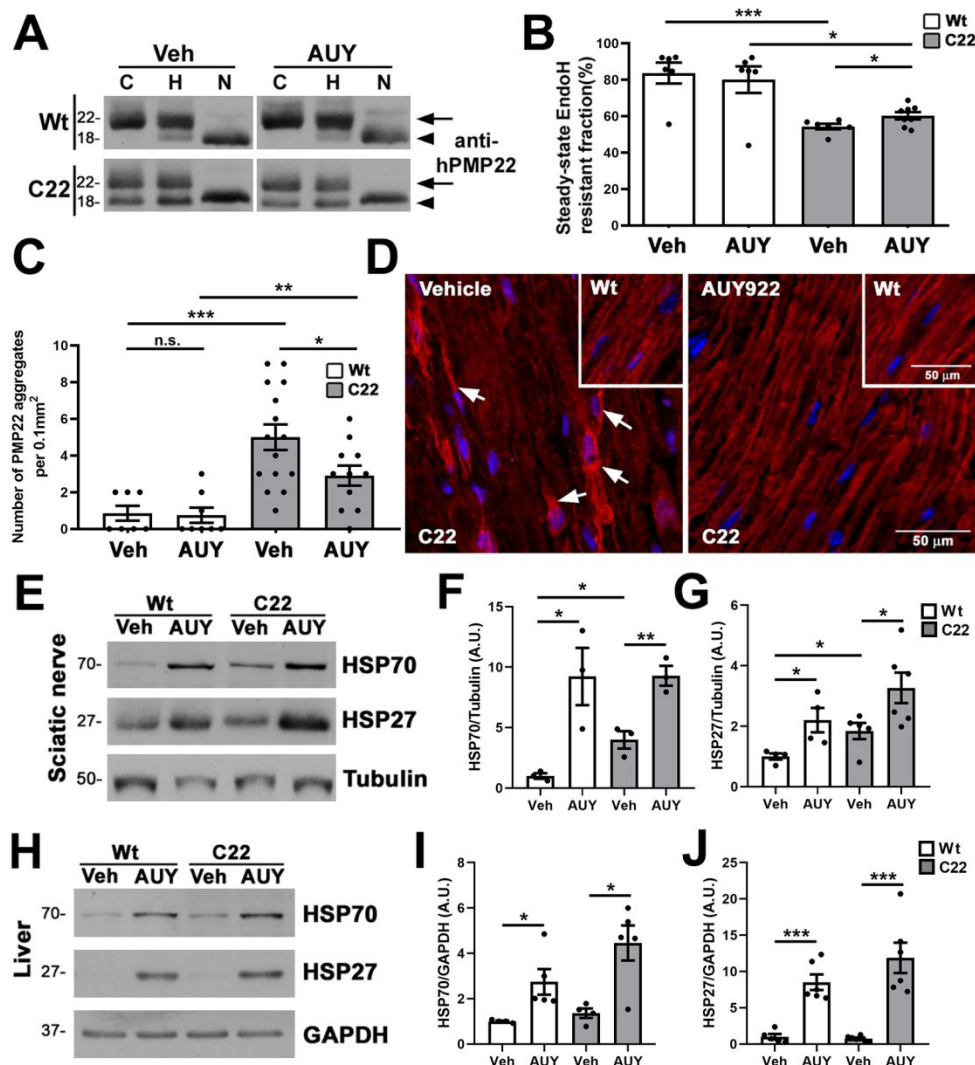
303

Subcellular Processing of PMP22 is Improved in AUY922-treated Neuropathic Mice

Previously, we showed impaired trafficking of the ectopic human PMP22, as indicated by a reduction in the endoglycosidase H (EndoH)-resistant protein fraction, in sciatic nerves of C22 mice¹³. To investigate whether the AUY922-associated improvements in nerve morphology and neuromuscular performance are linked with improved trafficking of PMP22, we subjected sciatic nerves to biochemical analyses (Figure 6A, B). In nerves from Wt mice, the EndoH-resistant fraction of PMP22 does not change upon AUY922 treatment (83.7 ± 5.7 Vs 80.0 ± 7.3). On the other hand, in samples from neuropathic mice we observed a significant AUY922-dependent increase (~11%) in the EndoH-resistant, membrane-associated PMP22 (54.3 ± 1.5 Vs 60.2 ± 1.9), indicating improved subcellular processing.

Mistrafficking of PMP22 within Schwann cells leads to cytosolic protein aggregation, a cellular phenotype previously observed in nerves from C22 animals^{13, 31}. To assess the effects of AUY922 administration on intracellular PMP22 aggregation, we stained longitudinal nerve sections with anti-PMP22 antibodies¹³. Quantification of PMP22-positive protein aggregates within a fixed field (0.1 mm²) identified an approximately 5-fold increase in samples from C22 vehicle-treated mice, as compared to Wt (Figure 6C). The frequency of protein aggregates is reduced by ~1.7-fold (5.0 ± 0.7 Vs 2.9 ± 0.9) upon AUY922 treatment, and is associated with improved myelin-like localization of PMP22 (Figure 6C, D). Note, with AUY922 administration, the PMP22-like immunostaining appears uniform, and is similar to nerves from Wt animals (insets in upper right corners). These results suggest that the improvements in nerve morphology are linked, in part, with enhanced processing of the overproduced PMP22.

Next, we confirmed the bioactivity of AUY922 by evaluating chaperone expression in the sciatic nerve (target tissue) and liver, where AUY922 is metabolized²³. We measured the levels of Hsp70 and Hsp27, as they are both regulated by HSF-1 (Figure 6E-J). In the sciatic nerves from drug-treated mice, the expression of HSP70 and HSP27 are increased, confirming the induction of the chaperone pathway in the target tissue (Figure 6E-G). Note, the baseline levels of HSP70 are increased in neuropathic samples as compared to Wt, a finding that is consistent with previous publications^{13, 32}. Similar to the nerve, quantification from independent western blots identifies significant increases in HSP70 and HSP27 in the liver of drug-injected mice, compared to the vehicle (Figure 6H-J). Therefore, as suggested by our previous studies with EC137, and in cells from HSP70-deficient mice^{15, 18}, HSP70 likely has a critical role in improving the processing of PMP22 and nerve morphology in samples from C22 mice (Figure 5, 6). Together, these results confirm the bioavailability and bioactivity of AUY922 in the sciatic nerve.



338
 339 **Figure 6. Improved processing of PMP22 in AUY922 treated C22 mice.** (A) Sciatic nerve
 340 lysates (5 μ g/lane) were treated with either EndoH (H) or PNGaseF (N) and probed with anti-
 341 human PMP22 antibodies. No enzyme samples served as controls (C). EndoH-resistant
 342 (arrows), and EndoH-sensitive (arrowheads) PMP22 fractions are marked. (B) Quantification of
 343 EndoH-resistant PMP22 fractions in sciatic nerves. (C) PMP22-positive aggregates per
 344 microscopic field (0.1 mm²) were counted in longitudinal sections of sciatic nerves. (D)
 345 Representative images of anti-PMP22 antibody stained (red) nerve sections from Wt (insets)
 346 and C22 mice are shown. Arrows mark PMP22-positive aggregates. Hoechst dye (blue) was
 347 used to visualize the nuclei. Scale bars, as shown. (E) Steady-state levels of HSP70 and
 348 HSP27 in vehicle (Veh) and AUY922 (AUY) treated nerve lysates (30 μ g/lane) were (F, G)
 349 quantified from independent western blots. (H) Whole liver lysates (30 μ g/lane) were processed
 350 for (I, J) HSP70 and HSP27 quantification. (E-J) GAPDH or Tubulin served as a loading control.
 351 Molecular mass on left in kDa. (B, C, F, G, I, J) n=3-8 mice per group and plotted as means \pm
 352 SEM; *** P <0.001; ** P <0.01; * P <0.05; n.s. non-significant; two-tailed Unpaired Student's t -test.

Improved Nerve Morphology in AUY922-treated TrJ Neuropathic Mice

Enhancements of chaperones by intermittent fasting or curcumin administration have shown benefits in TrJ neuropathic mice^{16, 33}. Further, functional HSP70 is critical in delivery of TrJ-PMP22 (L16P mutation) to the lysosomes for degradation¹⁸. Therefore, we evaluated AUY922 in cohorts of male and female TrJ mice; starting drug administration at 6 weeks of age. Nerves from vehicle-treated neuropathic mice show severe demyelination and axonal atrophy (Figure 7A, left), as described previously³⁴. In comparison, samples from the AUY922-treated group contain discernable myelinated axonal profiles and an improved overall nerve structure with larger caliber axons (Figure 7A, right).

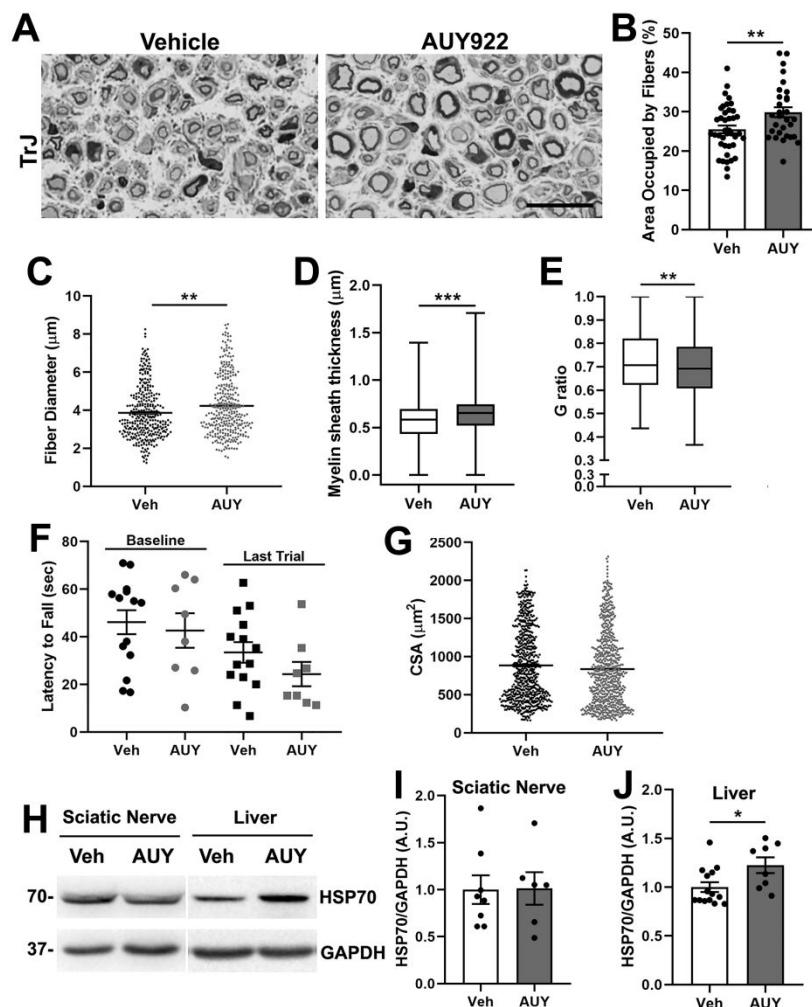


Figure 7. AUY922 promotes the maintenance of myelinated axons in TrJ mice. (A) Cross-sectional views of nerve sections from vehicle- (left) and AUY-treated (right) TrJ mice. Micron bar, 20 µm. (B-E) Morphometric analysis of nerves from vehicle and AUY-treated TrJ mice (n=4 mice, 320 fibers, 30-40 areas per group). (B) Percent area occupied by fibers, (C) fiber diameter, (D) myelin sheath thickness, and (E) G ratios were graphed. (F) Rotarod performance at baseline and at the end of treatment is shown for vehicle or AUY-treated TrJ mice. (G) Myofiber cross-sectional area of TA muscle from the indicated groups (n=5 mice, 695 fibers per group). (H) Sciatic nerve (30 µg/lane) and whole liver lysates (30 µg/lane), with (I, J) quantification, from vehicle (Veh) and AUY922 (AUY) treated TrJ mice, were assessed for

1
2
3 374 HSP70. (H-J) n=6-14 mice per group, with GAPDH serving as a loading control. Molecular mass
4 375 on left, in kDa. Graphs plotted as means (C, G) \pm SEM (B, F, I, J), or as whisker plots with
5 376 median (center line), quartiles (box), and extremes (whiskers) (D, E); *** P <0.001; ** P <0.01;
6 377 * P <0.05; two-tailed Unpaired Student's t -test.
7 378

8 379 We quantified these morphological measurements from vehicle and drug-treated TrJ
9 380 mice, and found statistically significant improvements in nerve tissue area occupied by fibers,
10 381 which correlates with an increase in nerve fiber diameter (Figure 7B, C). The thickness of myelin
11 382 around individual axons is also improved, leading to an overall improvement in nerve
12 383 myelination as reflected by a reduction in g-ratio (Figure 7D, E). However, we did not observe
13 384 any obvious improvements in the motor behavior or locomotion of AUY922-treated TrJ mice.
14 385 The rotarod data shown in Figure 7F is representative of several independent cohorts of mice
15 386 and indicates no treatment effect. In agreement, we failed to identify changes in TA myofiber
16 387 cross-sectional area upon drug treatment (Figure 7G).

17 388 For each mouse, we tested the bioactivity of the drug in target tissues by analyzing the
18 389 levels of HSP70 in nerve and liver, as above (Figure 6E-H). The levels of HSP70, which are
19 390 significantly elevated in TrJ neuropathic nerves as compared with Wt¹⁶, did not increase further
20 391 upon treatment with AUY922 (Figure 7H, I). In comparison, the liver of injected mice showed a
21 392 statistically significant increase in HSP70 upon AUY922 treatment (Figure 7H, J). Note, all
22 393 tissues were collected within 4-6 hours of the last drug injection to facilitate the detection of
23 394 bioactivity. Overall, the results from TrJ neuropathic mice indicate significant improvements in
24 395 nerve morphology, without detectable benefits in neuromuscular performance or TA myofiber
25 396 size.
26 397

27 398 DISCUSSION

28 399
29 400 In this study, we show enhanced neuromuscular function and improved peripheral nerve
30 401 morphology in AUY922-treated C22 neuropathic mice. These benefits are accompanied by
31 402 correction in the subcellular processing of the overexpressed, disease causing PMP22 protein.
32 403 In comparison, in the more severe, PMP22-mutant TrJ neuropathic mice the improvements in
33 404 nerve myelination failed to affect neuromuscular performance. Overall, the findings presented
34 405 here agree with other reports on the benefits of chaperone-inducing compounds in various
35 406 neurodegenerative conditions³⁵⁻³⁶. Further optimization of compound delivery, including dosage,
36 407 timing and route of administration may aid in improving drug efficacy in hereditary peripheral
37 408 neuropathies.

38 409 The benefits of HS pathway activation have been documented in various protein
39 410 misfolding disorders of the CNS^{1-3, 37-38}, however there have been fewer studies in the PNS.
40 411 Induction of the HS stress pathway, including increased expression of chaperones by a 5 month
41 412 long intermittent fasting regimen in TrJ mice, improved peripheral nerve morphology and
42 413 myelination¹⁶. Significantly, the improvements in nerve morphology were paralleled with
43 414 maintenance of motor performance, despite disease progression in ad libitum fed neuropathic
44 415 mice. A more direct correlation between the subcellular processing of PMP22 and chaperones
45 416 is evident from *in vitro* studies, where EC137, a synthetic HSP90 inhibitor, successfully
46 417 activated the HS pathway and improved myelination by Schwann cells from neuropathic C22
47 418 mice¹⁵. Due to the lack of availability of EC137, here we screened a set of commercially
48 419 available compounds, with similar pharmacological properties. Due to their anti-proliferative
49 420 properties, the potential effects of HSP90 inhibitors on cellular toxicity is of major concern³⁹,
50 421 particularly when chronic, long-term administration is needed. However, at lower dosages, these
51 422 drugs can robustly activate the stress pathways without cell death, which is beneficial for protein
52 423 misfolding diseases⁸.

1
2
3 424 Identification of the ideal therapeutic compound for hereditary peripheral neuropathies
4 425 poses specific challenges, as within a neuropathic nerve there is a heterogeneous population of
5 426 Schwann cells, with regards to differentiation state ⁴⁰. Initially, we selected low, nanomolar drug
6 427 concentration ranges in the MTS assay, which did not affect the viability of non-myelinating,
7 428 mitotic Schwann cells. In the context of myelination, which requires the differentiation of
8 429 Schwann cells, we identified AUY922 (100 nM) as the most effective drug in increasing myelin
9 430 synthesis, with BIIB021 closely behind (Figure 3). We tested both of these compounds in
10 431 cohorts of mice and found that oral administration of BIIB021 in neuropathic animals proved to
11 432 be a challenge, while i.p. injections with this compound gave inconsistent read out on bioactivity
12 433 in target nerve tissue. The mechanism for AUY922-mediated nerve improvement likely involved
13 434 HSP70, as this specific chaperone has been shown to alleviate protein aggregation in several
14 435 neurodegenerative diseases, including PMP22-associated neuropathies ^{4, 18, 37-38, 41}. Indeed,
15 436 HSP70 was robustly induced in the liver and nerve of drug treated C22 mice. A critical role for
16 437 HSP70 in our treatment paradigm is further supported by the study where crossing of HSP70-
17 438 knockout with TrJ mice exacerbated the neuropathic phenotype ⁴². Nonetheless, while AUY922
18 439 is considered to be a "classical HSP90 inhibitor" that upregulates HSP70 and HSP27, HSP90 α
19 440 knockdown studies in cultured cells indicate multiple targets ⁴³. Therefore, in addition to
20 441 inhibition of HSP90 and upregulation of HSP70 and HSP27, additional mechanisms may have
21 442 contributed to the beneficial effects of AUY922-treatment on neuropathic mice.

22 443
23 444 As originally described, C22 mice used in this study had strong phenotype within weeks
24 445 of birth, including unsteady gait and sudden reaction to loud noises ¹¹. Subsequently, the mice
25 446 developed distinct motor disabilities, with nerve demyelination and muscle atrophy by about 6
26 447 months of age ^{31, 44-45}. Our study was initiated at 7 weeks of age, as only at this age we detected
27 448 significant impairment of the C22 mice on the rotarod, as compared with age-matched Wt
28 449 littermates (Figure 5B). In our laboratory, we have been breeding the C22 mice for nearly 15
29 450 years and over time the animals became less phenotypic, and are now similar to what has been
30 451 described for the C3 mice ²⁶. Yet by genotyping we detect the human PMP22 transgene by
31 452 PCR, the copy number is unchanged from tissue banked from mice studied several years ago,
32 453 and the human protein is highly expressed ¹³. Still, these mildly affected C22 mice benefitted
33 454 from the AUY922 therapy, which we distinguished by improvements in both nerve and muscle
34 455 morphology. In comparison, the more severely affected TrJ mice only showed improvements in
35 456 nerve morphology without behavioral or skeletal muscle benefits. The difference in the
36 457 response of the C22 and TrJ mice to AUY922 therapy could be the results of underlying
37 458 developmental deficits in the neuromuscular system in TrJ that are refractory to HSP therapy ⁴⁶.
38 459 The heightened inflammation in nerves of TrJ mice, as compared to the C22 model ^{13, 47}, could
39 460 be an additional factor in impacting the response. Furthermore, at baseline, nerves from both
40 461 TrJ and C22 mice have elevated levels of HSP70 mice ³², however only the C22 samples we
41 462 detected a significant increase upon AUY922 treatment. The variance in drug effectiveness
42 463 could be the result of differences in drug metabolism, as well as the genetic defects, and
43 464 emphasize the need for optimization of drug therapies for the various forms of PMP22-linked
44 465 neuropathies, in mice and human.

45 466 Albeit the availability of animal models and advancements in the understanding of
46 467 CMT1A pathobiology, the therapeutic options for affected patients are limited. One of the
47 468 promising therapeutic candidates, ascorbic acid, elicited prominent improvement of the
48 469 neuropathic phenotype in C22 mice ¹², however it has failed in independently conducted clinical
49 470 trials ⁴⁸⁻⁴⁹. Progesterone antagonists are another class of therapeutic drugs which promoted
50 471 improvements in motor performance in rats that overexpress PMP22 ⁵⁰. The high toxicity, and
51 472 potential side effects of available progesterone antagonists however impeded further testing in
52 473 human clinical trials ⁵¹. Another small molecule, rapamycin, an activator of autophagy and an
53 474 immunosuppressant, improved myelin structure of TrJ sciatic nerves without significant benefits

1
2
3 474 in motor performance ⁴⁷. The rapamycin study emphasizes the potential distinct response of
4 475 nerve and muscle tissue to drugs, when using systemic administration. Besides natural and
5 476 engineered drugs, dietary supplements have been explored to alleviate neuropathic symptoms.
6 477 For example, curcumin, and more recently pyruvate supplementation in conjunction with NT-3
7 478 gene therapy, have shown benefits in improving nerve morphology and motor performance in
8 479 TrJ mice ^{33, 52}. Curcumin, which is known to work through the HSP70 pathway ⁴², could be
9 480 readily tested as a food supplement in CMT1A patients. Together, these preclinical studies in
10 481 rodents emphasize the need for stringent evaluation of potential drug candidates, preferably in
11 482 more than one independent animal models.

12 483 As of today, there have been two human clinical trials for CMT1A, both using orally
13 484 available molecules. The first trial tested ascorbic acid (vitamin C) to correct the expression of
14 485 the overproduced PMP22 ^{12, 53}, however this multicenter trial with nearly 500 CMT1A patients,
15 486 proved unsuccessful in providing benefits ⁴⁹. A recent international Phase 3 clinical trial for
16 487 CMT1A used pleiotropic drug therapy, including a low dose combination of baclofen, naltrexone,
17 488 and D-sorbitol ⁵⁴. Formal publication on the results from this clinical trial has not been made
18 489 public. In a recent study, PMP22 antisense oligonucleotides (ASOs) were utilized to treat C22
19 490 mice and CMT1A rats and reported a 50% reduction in the PMP22 mRNA, with significant
20 491 improvements in myelinated axons ⁵⁵. Therefore, an additional approach could involve the
21 492 combined use of small molecules, gene therapy, dietary supplements such as curcumin,
22 493 phospholipids and/or exercise. While the underlying subcellular pathogenesis of hereditary
23 494 demyelinating neuropathies is complex and might be significantly distinct across the genes
24 495 involved, the neuromuscular system has robust plasticity ⁵⁶, which aids repair. While
25 496 optimization of HSP90 inhibitor drug dosing and route of administration needs improvement for
26 497 efficacy, our results suggest that activation of the chaperone pathway alone, or in combination
27 498 with another therapeutic approach, may provide benefits in ameliorating the neuropathic
28 499 phenotype in affected individuals.

30 500 31 501 **METHODS**

32 502
33 503 **Mouse Colonies and Genotyping.** A founder pair of C22 mice (MGI: 2183770) obtained from
34 504 Dr. Clair Huxley ¹¹ were bred on C57Bl/6 or on CBA/CaJ background for multiple generations.
35 505 Heterozygous Trembler J (TrJ, MGI: 1856217) mice on a C57BL/6J background were bred to
36 506 wild type C57BL/6J mice, obtained from Jackson laboratories. All animals were maintained
37 507 under SPF conditions within the University of Florida animal care facilities and strictly in
38 508 compliance with procedures approved by the Institutional Animal Care and Use Committee
39 509 (IACUC). For genotyping C22 mice, DNA was obtained from tail biopsies of less than 8-day old
40 510 pups and analyzed by PCR using the following primer sets: C22- 5'
41 511 TTCTGCTGCCTGTGAGGAC 3' and 5' GGGTGAAGAGTTGGCAGAAG 3' which yield a 209 bp
42 512 product. The endogenous mouse PMP22 was identified using the following primers: 5'
43 513 GGTTGCCAAACTGGAGTGAT 3' and 5' CGGCTCTGTCAAGATTAGCC 3' yielding 458 bp
44 514 product. TrJ mice were genotyped as described ³⁴. At weaning age, littermates were segregated
45 515 by genotype and sex, and randomly assigned to vehicle and AUY922 treatment groups. All
46 516 efforts were made to reduce the number of animals used and to minimize their discomfort.

47 517
48 518 **Analysis of Transgene Copy Number and Genetic Background.** To investigate the milder
49 519 phenotype observed in our present colony of C22 mice, we analyzed the PMP22 transgene
50 520 copy number and the genetic background of the mice used in this study, in comparison to
51 521 archived material from ten years ago, when the phenotype more closely matched previous
52 522 reports. Liver was used as the source of genomic DNA, and QPCR was performed for the
53 523 human *PMP22* transgene using mouse *Pmp22* as an internal standard, as described ²⁶. Four

1
2
3 524 archived samples, and four samples from mice used in the present study, were analyzed. No
4 525 change in transgene copy number was detected between the two sets of tissue samples. As an
5 526 alternative explanation for the change in phenotype, we also examined the genetic background
6 527 of the mice using a panel of 48 SNP markers spanning the autosomes and X chromosome.
7 528 These markers are used routinely for genetic quality control at The Jackson Laboratory. This
8 529 analysis revealed that the archived samples were a mix of C57BL/6J and C57BL/6N genetic
9 530 backgrounds, whereas the mice used in the current study were predominantly CBA/Ca, but still
10 531 carried some heterozygous C57BL/6 alleles on a subset of chromosomes. Based on these
11 532 analyses, we conclude the change in phenotype is due to the change in genetic background.
12 533 However, as all studies described here used contemporaneous littermate controls and did not
13 534 rely on historical data for comparison, this does not influence the interpretation of our results.
14 535

15 536 **Cell Culture Models.** Non-myelinating Schwann cell cultures were established from the sciatic
16 537 nerves of postnatal day 2 rats, as described ¹⁰. The cells were maintained in DMEM (Gibco,
17 538 Thermo Fisher, Waltham, MA) and supplemented with 10% FCS (HyClone, Thermo Fisher),
18 539 100 µg/ml bovine pituitary extract (Biomedical Technologies Inc., Stoughton, MA) and 5 µM
20 540 forskolin (Calbiochem, Millipore, Burlington, MA). Dorsal-Root Ganglion (DRG) explants were
21 541 established from embryonic day 12-13 Wt and C22 embryos ¹⁵. Briefly, DRGs were dissociated
22 542 in 0.25% trypsin (Gibco) and plated onto collagen-coated cell culture wells. DNA isolated from
23 543 each embryo was used for genotyping, as described above. All explants were maintained in
24 544 MEM (Gibco), 10% FCS (Hyclone), 0.3% glucose (Sigma-Aldrich, St. Louis, MO), 10 mM
25 545 HEPES (Gibco) and 100 ng/ml nerve growth factor (Harlan Bioproducts for Science,
26 546 Indianapolis, IN) for 7 days. The cultures were then supplemented with 50 µg/ml ascorbate for
27 547 additional 7 days to promote myelin formation. For Schwann cell-depleted neuronal cultures,
28 548 explants were subjected to alternate-day treatment with 5-fluoro-2'-deoxyuridine (FUdR) for 10
29 549 days and then continued on the same paradigm described above ¹⁵.
30 550

31 551 ***In vitro* Pharmacologic Treatment Paradigms.** HSP90 inhibitor compounds, including
32 552 AT13387 (S1163), AUY922 (S1069), BIIB021 (S1175), SNX5422 (S2656), STA9090 (S1159),
33 553 were purchased from Selleckchem (Houston, TX) and stored at a stock concentration of 1 mM
34 554 in DMSO. Primary Schwann cells were treated with HSP90 inhibitors at the indicated
35 555 concentrations in complete media (see above), 24 h after seeding. DMSO served as the vehicle
36 556 control while geldanamycin (GA) was used as a positive control for heat shock pathway
37 557 activation. The DRG explant cultures were maintained for 7 days in ascorbate-containing media
38 558 prior to treatment with either DMSO, AUY922 (100 nM) or BIIB021 (100 nM), every third day (72
39 559 h apart). Twenty-four hours after the third treatment, cultures were procured for either
40 560 biochemical or immunochemical analyses ¹⁵.
41 561

42 562 **Cell Viability Assay.** Schwann cells were plated at a seeding density of 10⁴ cells/well in a 96-
43 563 well plate (Nunc, Thermo Fisher), coated with poly-L-lysine (Sigma), and treated either with
44 564 DMSO or an HSP90 inhibitor at the desired concentrations for 24 h ¹⁵. At the end of the
45 565 treatment, cells were incubated in a mixture of MTS (3-(4, 5-dimethylthiazol-2-yl)-5-(3-
46 566 carboxymethoxyphenyl)-2-(4-sulfophenyl)-2H-tetrazolium) (333 µg/ml) and phenazine
47 567 methosulfate (25 µM) for 2 h at 37°C, producing the soluble formazan product (Promega,
48 568 Madison, WI). The formazan product was measured spectrophotometrically at 490 nm and
49 569 graphed as percent of DMSO-treated controls using GraphPad Prism v5.0 software.
50 570

51 571 **Quantitative RT-PCR.** Rat Schwann cells, treated with either DMSO or the selected HSP90
52 572 inhibitor compounds (100 nM) were harvested in TRIzol (Invitrogen, Carlsbad, CA) and RNA

1
2
3 573 was isolated as per the manufacturer's instructions. One microgram of total RNA was used to
4 574 synthesize cDNA using the SuperScript III first strand synthesis kit (Invitrogen). The same
5 575 volume of undiluted cDNA from each sample was used for real time (RT) PCR analysis, using
6 576 the SYBR GreenER qPCR kit (Invitrogen) and QuantiTect Primer for HSP70 (QT00370489) or
7 577 GAPDH (QT00199633). The normalized transcript levels of HSP70 relative to geldanamycin
8 578 (GA) were determined using the $2^{-\Delta\Delta CT}$ method⁵⁷. Values obtained were analyzed and graphed
9 579 with the help of GraphPad Prism v5.0 software.
10 580

11 581 **AUY922 Administration, Rotarod Testing, and Serum and Liver Analyses.** During the
12 582 course of the study, the body weight of each mouse was recorded twice per week. Baseline
13 583 rotarod measurements were obtained before the start of the compound treatment at 12 weeks
14 584 of age for C22, and at 6 weeks of age for TrJ mice. The mice were trained the first two days at 5
15 585 rpm for 60 sec; three trials/day, with 30 min breaks¹⁶. On the third day, mice were tested on the
16 586 rotarod, accelerating from 16 rpm to 36 rpm in steps of 4 rpm increase/min⁴². The control
17 587 groups were injected intraperitoneal (i.p.) twice/week with the vehicle consisting of 10% DMSO,
18 588 5% Tween-20 and 85% saline²³. The treatment groups received 2 mg/kg AUY922, using the
19 589 same route and vehicle for administration. Dosage for AUY922 was determined based on the
20 590 half-life of the compound in plasma²³ and results of the in vitro experiments (see Figures 2 and
21 591 3). Rotarod testing was done on all groups monthly, where all mice underwent the same 3-day
22 592 testing. The time on the rotarod before falling was recorded for each mouse and graphed. The
23 593 study was terminated after 20 weeks of drug treatment. At termination, the mice were sacrificed
24 594 within 4 hours after the final injection and blood and tissue samples were collected. Blood was
25 595 collected into tubes with clot activator gel (BD 365967, Franklin Lakes, NJ), and centrifuged at
26 596 10,000 rpm for five minutes to isolate serum. Serum and liver samples were sent to Charles
27 597 River Laboratories (Wilmington, MA) for processing and analysis of AUY922 concentration via
28 598 protein precipitation, followed by LC-MS/MS using Glafenine and Carbamazepine as internal
29 599 standards.
30 600

31 601 **In situ Isometric Twitch Torque Analyses.** Isometric twitch torque analysis was performed on
32 602 the tibialis anterior (TA) muscle and anterior tibial tendon. Under anesthesia, the skin and fascia
33 603 surrounding the distal hindlimb were surgically removed exposing the TA. Braided (4-0) silk
34 604 surgical suture (Teleflex Medical, Wayne, PA) was secured around the anterior tibial tendon
35 605 before all tendons to the foot were detached. Mice were positioned in dorsal recumbence on a
36 606 pre-heated physiology table to maintain body temperature at 37°C. A clamp was used to secure
37 607 the hindlimb at 90° at the knee and the paw was positioned to the physiology table using
38 608 transpore surgical tape (3M). The anterior tibial tendon was secured to a 300C-LR-FP muscle
39 609 lever (Aurora Scientific, Aurora, ON, Canada). Cathode and anode electrodes were inserted
40 610 distal to the fibular to stimulate the peroneal nerve. Under control of the Dynamic Muscle
41 611 Control (DMC) and Analysis (DMA) Software suite (Aurora Scientific), optimal electrode
42 612 placement was determined by repositioning of the electrodes and stimulating the nerve at 1Hz
43 613 until maximum twitch amplitude was recorded for a given position. Optimal length-tension was
44 614 determined by performing isometric twitch stimulation (2500 Hz) at an increasing range of
45 615 amplitudes and tensions until maximum twitch amplitude was observed. Three successive
46 616 tetanic stimulations (200Hz, 100 pulses per train, 60s between independent stimuli) were
47 617 performed and the muscle was allowed resting for 5 minutes. Single stimulations at 15Hz,
48 618 30Hz, 60Hz, 100Hz, 120Hz, 160Hz and 200Hz were then performed with 30s between each
49 619 successive frequency and the resulting torque was recorded and analyzed using DMC and DMA
50 620 (Aurora Scientific).
51 621

52 622 **Western Blot Analyses.** Cell harvesting and tissue homogenization was done in sodium
53
54
55

1
2
3 623 dodecyl sulfate (SDS) gel sample buffer (62.5 mM Tris pH 6.8, 10% glycerol, 3% SDS),
4 624 supplemented with protease and phosphatase inhibitors¹⁵. Protein concentrations were
5 625 measured using BCA assay (Pierce, Thermo Fisher). Digestions using endoglycosidase H
6 626 (EndoH) or N-glycosidase F (PNGaseF) enzymes (New England Biolabs) were performed to
7 627 assess the subcellular processing of PMP22, as described⁵⁸. Equal amounts of proteins for
8 628 each experiment were separated on denaturing SDS gels and transferred to nitrocellulose
9 629 membrane (0.45 μm or 0.22 μm pore size) (Bio-Rad, Hercules, CA). Membranes were blocked
10 630 in 5% milk (in Tris-buffered saline with 0.05% Tween-20) and incubated with the indicated
11 631 primary antibodies (Table 1) overnight at 4°C. Bound antibodies were detected with anti-rabbit,
12 632 anti-goat, anti-mouse IgG or anti-chicken IgY HRP-linked secondary antibodies (Sigma) and
13 633 visualized with the chemiluminescence detection method (Perkin-Elmer Life Sciences, Waltham,
14 634 MA). Films were digitally imaged using a GS-800 densitometer (Bio-Rad) and were formatted
15 635 for printing, using Adobe Photoshop.

16 636
17 637 **Immunostaining.** Explant cultures were fixed in 4% paraformaldehyde (EMS, Hatfield, PA) and
18 638 permeabilized in 100% ice-cold methanol (Fisher Scientific, Hampton, NH). After blocking with
19 639 5% normal goat serum, samples were incubated with anti-MBP antibodies, overnight at 4°C.
20 640 Bound antibodies were detected with Alexa Fluor 488 goat anti-rat IgG (Molecular Probes,
21 641 Eugene, OR). Coverslips were mounted using the Prolong Antifade kit (Molecular Probes).
22 642 Proximal regions of sciatic nerves were sectioned (5 μm thickness) and processed for
23 643 immunostaining with anti-PMP22 antibodies, as described¹³. AlexaFluor 594-conjugated goat
24 644 anti-rabbit antibodies were used to detect the bound primary antibodies. Samples which were
25 645 processed in parallel without incubation with primary antibodies served as the negative controls.
26 646 Images were obtained using a SPOT digital camera (Diagnostic Instrumentals, Sterling Heights,
27 647 MI), with a Nikon Eclipse E800 or an Olympus DSU spinning disc confocal (Tokyo, Japan)
28 648 microscope, using identical exposure settings. Images were processed using Photoshop (Adobe
29 649 Systems).

30 650
31 651 **Myelin Internode Length Measurement.** DRG cultures were stained for MBP as described
32 652 above, to label myelin internode segments. The MBP-positive internodes were measured using
33 653 ImageJ software (NIH). Measurements from three independent experiments, per treatment per
34 654 genotype, were graphed using GraphPad Prism software.

35 655
36 656 **Morphometric Analyses of Sciatic Nerve.** Proximal ends of sciatic nerves from vehicle and
37 657 AUY922-treated groups were fixed by immersion in ice-cold 2% paraformaldehyde and 2%
38 658 glutaraldehyde, in 0.1 M sodium cacodylate buffer at 4°C⁵⁹. Plastic sections, stained with
39 659 toluidine blue were prepared by the Robert P. Apkarian Integrated Electron Microscopy Core at
40 660 Emory University, and imaged with a light microscope (Zeiss Axioscop 2 plus). Axon diameter,
41 661 fiber diameter, myelin sheath thickness (n=320-1100 fibers per group), and total area occupied
42 662 by nerve fibers (n=20-40 areas per group) were measured using ImageJ software (NIH)¹⁶. G-
43 663 ratio was calculated as axon diameter/ fiber diameter, using the respective values. Myelin
44 664 sheath thickness was calculated as [(fiber perimeter – axon perimeter) / 2 π]⁶⁰.

45 665
46 666 **Cross-sectional Area Analyses of TA Muscles.** Fresh-frozen TA muscles from C22 and TrJ
47 667 mice, treated with vehicle or AUY922, were sectioned at 10 μm thickness and immunostained
48 668 with rabbit anti-laminin antibody to outline the individual myofibers. AlexaFluor 488-conjugated
49 669 goat anti-rabbit secondary antibody was used to detect the bound primary antibody, and
50 670 Hoechst was used to label nuclei. Images were captured using a Nikon DS digital camera fitted
51 671 on a Nikon Eclipse E800 microscope. Myofiber cross-sectional areas of individual fibers were
52 672 measured using ImageJ software (NIH) and exported to GraphPad Prism v8.0.1 for analysis.

1
2
3 673
4 674 **Data analyses.** For all comparisons, mean \pm S.E.M was calculated and statistical differences
5 675 were determined using unpaired two-tailed Student's *t*-test. *P*-values <0.05 (*), <0.01 (**),
6 676 <0.001 (***) were considered to be significant. For *in situ* torque analysis, significance was
7 677 determined using two-way ANOVA with Sidak's multiple comparison between individual groups
8 678 and frequencies. For longitudinal rotarod analysis, significance was determined using two-way
9 679 ANOVA with Fisher's LSD *post hoc* test.
10 680

Table 1: Primary antibodies used in this study.

Species	Antigen	Source and Catalog #	Dilution	
			WB	IS
Rabbit	HSP70	Stressgen; SPA-812	1:3000	n/a
Rabbit	HSP70	Abcam; ab137680	1:2000	n/a
Goat	HSP27	Santa Cruz Biotechnology, Inc.; sc-1049	1:1000	n/a
Mouse	GAPDH	Encor Biotechnology Inc.; MCA-1D4	1:10000	n/a
Rabbit	GAPDH	Encor Biotechnology Inc.; RPCA-GAPDH	1:8000	n/a
Mouse	Tubulin	Sigma, St Louis, MO, USA ; T6199	1:2000	n/a
Mouse	Tubulin	Encor Biotechnology Inc.; MCA-1B12	1:10000	n/a
Chicken	P0	Encor Biotechnology Inc.	1:500	n/a
Rat	MBP	Chemicon; MAB386	n/a	1:500
Rabbit	PMP22	Chittoor et al., 2013	1:1000	1:250
Rabbit	Laminin	Sigma; L9393	n/a	1:300

WB: Western Blotting. IS: Immunostaining. n/a: not applicable

Author Contributions:

Research design: VC, LN. Experimental work: VC, HB, AT, DF, KM, RB, LN. Data analyses and interpretation: VC, HB, AT, DF, KM, RB, TF, LN. Writing, review, and revision of the manuscript: VC, HB, AT, DF, RB, TF, LN.

Acknowledgements: We thank members of the Notterpek lab for assistance with various technical aspects of this project over a 3 year period, including genotyping, and weighing the mice, behavioral testing, morphological studies and sample collection. We acknowledge the Robert P. Apkarian Integrated Electron Microscopy Core at Emory University for semithin sectioning and toluidine blue processing of sciatic nerves, and Greg Ballard for help with the SNP genome scan. This project was supported by NIH-NINDS grants NS091435 (LN) and NS098523 (RWB).

References

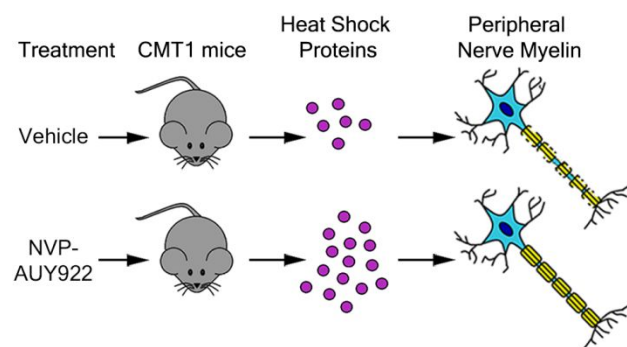
1. Jiang, Y. Q.; Wang, X. L.; Cao, X. H.; Ye, Z. Y.; Li, L.; Cai, W. Q., Increased heat shock transcription factor 1 in the cerebellum reverses the deficiency of Purkinje cells in Alzheimer's disease. *Brain Res* **2013**, *1519*, 105-11.
2. Lin, P. Y.; Simon, S. M.; Koh, W. K.; Folorunso, O.; Umbaugh, C. S.; Pierce, A., Heat shock factor 1 over-expression protects against exposure of hydrophobic residues on mutant SOD1 and early mortality in a mouse model of amyotrophic lateral sclerosis. *Mol Neurodegener* **2013**, *8*, 43.
3. Kalmar, B.; Lu, C. H.; Greensmith, L., The role of heat shock proteins in Amyotrophic Lateral Sclerosis: The therapeutic potential of Arimoclomol. *Pharmacol Ther* **2014**, *141* (1), 40-54.
4. Jinwal, U. K.; Akoury, E.; Abisambra, J. F.; O'Leary, J. C., 3rd; Thompson, A. D.; Blair, L. J.; Jin, Y.; Bacon, J.; Nordhues, B. A.; Cockman, M.; Zhang, J.; Li, P.; Zhang, B.; Borysov, S.; Uversky, V. N.; Biernat, J.; Mandelkow, E.; Gestwicki, J. E.; Zweckstetter, M.; Dickey, C. A., Imbalance of Hsp70 family variants fosters tau accumulation. *Faseb J* **2013**, *27* (4), 1450-9.
5. Mattoo, R. U.; Sharma, S. K.; Priya, S.; Finka, A.; Goloubinoff, P., Hsp110 is a bona fide chaperone using ATP to unfold stable misfolded polypeptides and reciprocally collaborate with Hsp70 to solubilize protein aggregates. *J Biol Chem* **2013**, *288* (29), 21399-411.
6. Sancho, M.; Herrera, A. E.; Orzaez, M.; Perez-Paya, E., Inactivation of Apaf1 reduces the formation of mutant huntingtin-dependent aggregates and cell death. *Neuroscience* **2014**, *262*, 83-91.
7. Ali, A.; Bharadwaj, S.; O'Carroll, R.; Ovsenek, N., HSP90 interacts with and regulates the activity of heat shock factor 1 in *Xenopus* oocytes. *Mol Cell Biol* **1998**, *18* (9), 4949-60.
8. Westerheide, S. D.; Morimoto, R. I., Heat shock response modulators as therapeutic tools for diseases of protein conformation. *J Biol Chem* **2005**, *280* (39), 33097-100.
9. Lupski, J. R.; Garcia, C. A., Molecular genetics and neuropathology of Charcot-Marie-Tooth disease type 1A. *Brain Pathol* **1992**, *2* (4), 337-49.
10. Notterpek, L.; Ryan, M. C.; Tobler, A. R.; Shooter, E. M., PMP22 accumulation in aggresomes: implications for CMT1A pathology. *Neurobiol Dis* **1999**, *6* (5), 450-60.
11. Huxley, C.; Passage, E.; Manson, A.; Putzu, G.; Figarella-Branger, D.; Pellissier, J. F.; Fontes, M., Construction of a mouse model of Charcot-Marie-Tooth disease type 1A by pronuclear injection of human YAC DNA. *Hum Mol Genet* **1996**, *5* (5), 563-9.
12. Passage, E.; Norreel, J. C.; Noack-Fraissignes, P.; Sanguedolce, V.; Pizant, J.; Thirion, X.; Robaglia-Schlupp, A.; Pellissier, J. F.; Fontes, M., Ascorbic acid treatment corrects the phenotype of a mouse model of Charcot-Marie-Tooth disease. *Nat Med* **2004**, *10* (4), 396-401.
13. Chittoor, V. G.; Sooyeon, L.; Rangaraju, S.; Nicks, J. R.; Schmidt, J. T.; Madorsky, I.; Narvaez, D. C.; Notterpek, L., Biochemical characterization of protein quality control mechanisms during disease progression in the C22 mouse model of CMT1A. *ASN Neuro* **2013**, *5* (5), e00128.

- 1
2
3 14. Fortun, J.; Dunn, W. A., Jr.; Joy, S.; Li, J.; Notterpek, L., Emerging role for
4 autophagy in the removal of aggresomes in Schwann cells. *J Neurosci* **2003**, *23* (33),
5 10672-80.
6
7 15. Rangaraju, S.; Madorsky, I.; Pileggi, J. G.; Kamal, A.; Notterpek, L.,
8 Pharmacological induction of the heat shock response improves myelination in a
9 neuropathic model. *Neurobiol Dis* **2008**, *32* (1), 105-15.
10
11 16. Madorsky, I.; Opalach, K.; Waber, A.; Verrier, J. D.; Solmo, C.; Foster, T.; Dunn,
12 W. A., Jr.; Notterpek, L., Intermittent fasting alleviates the neuropathic phenotype in a
13 mouse model of Charcot-Marie-Tooth disease. *Neurobiol Dis* **2009**, *34* (1), 146-54.
14
15 17. Opalach, K.; Rangaraju, S.; Madorsky, I.; Leeuwenburgh, C.; Notterpek, L.,
16 Lifelong calorie restriction alleviates age-related oxidative damage in peripheral nerves.
17 *Rejuvenation Res* **2010**, *13* (1), 65-74.
18
19 18. Chittoor-Vinod, V. G.; Lee, S.; Judge, S. M.; Notterpek, L., Inducible HSP70 is
20 critical in preventing the aggregation and enhancing the processing of PMP22. *ASN*
21 *Neuro* **2015**, *7* (1).
22
23 19. Urban, M. J.; Pan, P.; Farmer, K. L.; Zhao, H.; Blagg, B. S.; Dobrowsky, R. T.,
24 Modulating molecular chaperones improves sensory fiber recovery and mitochondrial
25 function in diabetic peripheral neuropathy. *Exp Neurol* **2012**, *235* (1), 388-96.
26
27 20. Zhang, X.; Li, C.; Fowler, S. C.; Zhang, Z.; Blagg, B. S. J.; Dobrowsky, R. T.,
28 Targeting Heat Shock Protein 70 to Ameliorate c-Jun Expression and Improve
29 Demyelinating Neuropathy. *ACS Chem Neurosci* **2018**, *9* (2), 381-390.
30
31 21. Miyata, Y., Hsp90 inhibitor geldanamycin and its derivatives as novel cancer
32 chemotherapeutic agents. *Curr Pharm Des* **2005**, *11* (9), 1131-8.
33
34 22. Saibil, H., Chaperone machines for protein folding, unfolding and disaggregation.
35 *Nat Rev Mol Cell Biol* **2013**, *14* (10), 630-42.
36
37 23. Eccles, S. A.; Massey, A.; Raynaud, F. I.; Sharp, S. Y.; Box, G.; Valenti, M.;
38 Patterson, L.; de Haven Brandon, A.; Gowan, S.; Boxall, F.; Aherne, W.; Rowlands, M.;
39 Hayes, A.; Martins, V.; Urban, F.; Boxall, K.; Prodromou, C.; Pearl, L.; James, K.;
40 Matthews, T. P.; Cheung, K. M.; Kalusa, A.; Jones, K.; McDonald, E.; Barril, X.; Brough,
41 P. A.; Cansfield, J. E.; Dymock, B.; Drysdale, M. J.; Finch, H.; Howes, R.; Hubbard, R.
42 E.; Surgenor, A.; Webb, P.; Wood, M.; Wright, L.; Workman, P., NVP-AUY922: a novel
43 heat shock protein 90 inhibitor active against xenograft tumor growth, angiogenesis, and
44 metastasis. *Cancer Res* **2008**, *68* (8), 2850-60.
45
46 24. Hickey, M. A.; Zhu, C.; Medvedeva, V.; Lerner, R. P.; Patassini, S.; Franich, N.
47 R.; Maiti, P.; Frautschy, S. A.; Zeitlin, S.; Levine, M. S.; Chesselet, M. F., Improvement
48 of neuropathology and transcriptional deficits in CAG 140 knock-in mice supports a
49 beneficial effect of dietary curcumin in Huntington's disease. *Mol Neurodegener* **2012**, *7*,
50 12.
51
52 25. Zhang, Y.; Bokov, A.; Gelfond, J.; Soto, V.; Ikeno, Y.; Hubbard, G.; Diaz, V.;
53 Sloane, L.; Maslin, K.; Treaster, S.; Rendon, S.; van Remmen, H.; Ward, W.; Javors,
54 M.; Richardson, A.; Austad, S. N.; Fischer, K., Rapamycin extends life and health in
55 C57BL/6 mice. *J Gerontol A Biol Sci Med Sci* **2014**, *69* (2), 119-30.
56
57 26. Verhamme, C.; King, R. H.; ten Asbroek, A. L.; Muddle, J. R.; Nourallah, M.;
58 Wolterman, R.; Baas, F.; van Schaik, I. N., Myelin and axon pathology in a long-term
59 study of PMP22-overexpressing mice. *J Neuropathol Exp Neurol* **2011**, *70* (5), 386-98.
60

- 1
2
3 27. Huguet, A.; Medja, F.; Nicole, A.; Vignaud, A.; Guiraud-Dogan, C.; Ferry, A.;
4 Decostre, V.; Hogrel, J. Y.; Metzger, F.; Hoeflich, A.; Baraibar, M.; Gomes-Pereira, M.;
5 Puymirat, J.; Bassez, G.; Furling, D.; Munnich, A.; Gourdon, G., Molecular,
6 physiological, and motor performance defects in DMSXL mice carrying >1,000 CTG
7 repeats from the human DM1 locus. *PLoS Genet* **2012**, *8* (11), e1003043.
- 8 28. Falk, D. J.; Todd, A. G.; Lee, S.; Soustek, M. S.; ElMallah, M. K.; Fuller, D. D.;
9 Notterpek, L.; Byrne, B. J., Peripheral nerve and neuromuscular junction pathology in
10 Pompe disease. *Hum Mol Genet* **2015**, *24* (3), 625-36.
- 11 29. Todd, A. G.; McElroy, J. A.; Grange, R. W.; Fuller, D. D.; Walter, G. A.; Byrne, B.
12 J.; Falk, D. J., Correcting Neuromuscular Deficits With Gene Therapy in Pompe
13 Disease. *Ann Neurol* **2015**, *78* (2), 222-34.
- 14 30. Huxley, C.; Passage, E.; Robertson, A. M.; Youl, B.; Huston, S.; Manson, A.;
15 Saberán-Djoniedi, D.; Figarella-Branger, D.; Pellissier, J. F.; Thomas, P. K.; Fontes, M.,
16 Correlation between varying levels of PMP22 expression and the degree of
17 demyelination and reduction in nerve conduction velocity in transgenic mice. *Hum Mol*
18 *Genet* **1998**, *7* (3), 449-58.
- 19 31. Fortun, J.; Go, J. C.; Li, J.; Amici, S. A.; Dunn, W. A., Jr.; Notterpek, L.,
20 Alterations in degradative pathways and protein aggregation in a neuropathy model
21 based on PMP22 overexpression. *Neurobiol Dis* **2006**, *22* (1), 153-64.
- 22 32. Amici, S. A.; Dunn, W. A., Jr.; Notterpek, L., Developmental abnormalities in the
23 nerves of peripheral myelin protein 22-deficient mice. *J Neurosci Res* **2007**, *85* (2), 238-
24 49.
- 25 33. Khajavi, M.; Shiga, K.; Wiszniewski, W.; He, F.; Shaw, C. A.; Yan, J.; Wensel, T.
26 G.; Snipes, G. J.; Lupski, J. R., Oral curcumin mitigates the clinical and neuropathologic
27 phenotype of the Trembler-J mouse: a potential therapy for inherited neuropathy. *Am J*
28 *Hum Genet* **2007**, *81* (3), 438-53.
- 29 34. Notterpek, L.; Shooter, E. M.; Snipes, G. J., Upregulation of the endosomal-
30 lysosomal pathway in the trembler-J neuropathy. *J Neurosci* **1997**, *17* (11), 4190-200.
- 31 35. Li, C.; Ma, J.; Zhao, H.; Blagg, B. S.; Dobrowsky, R. T., Induction of heat shock
32 protein 70 (Hsp70) prevents neuregulin-induced demyelination by enhancing the
33 proteasomal clearance of c-Jun. *ASN Neuro* **2012**, *4* (7), e00102.
- 34 36. Ciechanover, A.; Kwon, Y. T., Protein Quality Control by Molecular Chaperones
35 in Neurodegeneration. *Front Neurosci* **2017**, *11*, 185.
- 36 37. Hoshino, T.; Murao, N.; Namba, T.; Takehara, M.; Adachi, H.; Katsuno, M.;
37 Sobue, G.; Matsushima, T.; Suzuki, T.; Mizushima, T., Suppression of Alzheimer's
38 disease-related phenotypes by expression of heat shock protein 70 in mice. *J Neurosci*
39 **2011**, *31* (14), 5225-34.
- 40 38. Gifondorwa, D. J.; Jimenez-Moreno, R.; Hayes, C. D.; Rouhani, H.; Robinson, M.
41 B.; Strupe, J. L.; Caress, J.; Milligan, C., Administration of Recombinant Heat Shock
42 Protein 70 Delays Peripheral Muscle Denervation in the SOD1(G93A) Mouse Model of
43 Amyotrophic Lateral Sclerosis. *Neurol Res Int* **2012**, *2012*, 170426.
- 44 39. Evans, C. G.; Chang, L.; Gestwicki, J. E., Heat shock protein 70 (hsp70) as an
45 emerging drug target. *J Med Chem* **2010**, *53* (12), 4585-602.
- 46
47
48
49
50
51
52
53
54
55
56
57
58
59
60

- 1
2
3 40. Juneja, M.; Burns, J.; Saporta, M. A.; Timmerman, V., Challenges in modelling
4 the Charcot-Marie-Tooth neuropathies for therapy development. *J Neurol Neurosurg*
5 *Psychiatry* **2019**, *90* (1), 58-67.
- 6 41. Bobkova, N. V.; Garbuz, D. G.; Nesterova, I.; Medvinskaya, N.; Samokhin, A.;
7 Alexandrova, I.; Yashin, V.; Karpov, V.; Kukharsky, M. S.; Ninkina, N. N.; Smirnov, A.
8 A.; Nudler, E.; Evgen'ev, M., Therapeutic effect of exogenous hsp70 in mouse models
9 of Alzheimer's disease. *J Alzheimers Dis* **2014**, *38* (2), 425-35.
- 10 42. Okamoto, Y.; Pehlivan, D.; Wiszniewski, W.; Beck, C. R.; Snipes, G. J.; Lupski, J.
11 R.; Khajavi, M., Curcumin facilitates a transitory cellular stress response in Trembler-J
12 mice. *Hum Mol Genet* **2013**, *22* (23), 4698-705.
- 13 43. Wang, Y.; Koay, Y. C.; McAlpine, S. R., Redefining the Phenotype of Heat Shock
14 Protein 90 (Hsp90) Inhibitors. *Chemistry* **2017**, *23* (9), 2010-2013.
- 15 44. Norreel, J. C.; Vinay, L.; Fontes, M.; Clarac, F., Close relationship between motor
16 impairments and loss of functional motoneurons in a Charcot-Marie-Tooth type 1A
17 model. *Neuroscience* **2003**, *116* (3), 695-703.
- 18 45. Szigeti, K.; Lupski, J. R., Charcot-Marie-Tooth disease. *Eur J Hum Genet* **2009**,
19 *17* (6), 703-10.
- 20 46. Scurry, A. N.; Heredia, D. J.; Feng, C. Y.; Gephart, G. B.; Hennig, G. W.; Gould,
21 T. W., Structural and Functional Abnormalities of the Neuromuscular Junction in the
22 Trembler-J Homozygote Mouse Model of Congenital Hypomyelinating Neuropathy. *J*
23 *Neuropathol Exp Neurol* **2016**, *75* (4), 334-46.
- 24 47. Nicks, J.; Lee, S.; Harris, A.; Falk, D. J.; Todd, A. G.; Arredondo, K.; Dunn, W. A.,
25 Jr.; Notterpek, L., Rapamycin improves peripheral nerve myelination while it fails to
26 benefit neuromuscular performance in neuropathic mice. *Neurobiol Dis* **2014**, *70*, 224-
27 36.
- 28 48. Pareyson, D.; Reilly, M. M.; Schenone, A.; Fabrizi, G. M.; Cavallaro, T.; Santoro,
29 L.; Vita, G.; Quattrone, A.; Padua, L.; Gemignani, F.; Visioli, F.; Laura, M.; Radice, D.;
30 Calabrese, D.; Hughes, R. A.; Solari, A., Ascorbic acid in Charcot-Marie-Tooth disease
31 type 1A (CMT-TRIAAL and CMT-TRAUK): a double-blind randomised trial. *Lancet*
32 *Neurol* **2011**, *10* (4), 320-8.
- 33 49. Lewis, R. A.; McDermott, M. P.; Herrmann, D. N.; Hoke, A.; Clawson, L. L.;
34 Siskind, C.; Feely, S. M.; Miller, L. J.; Barohn, R. J.; Smith, P.; Luebke, E.; Wu, X.; Shy,
35 M. E., High-dosage ascorbic acid treatment in Charcot-Marie-Tooth disease type 1A:
36 results of a randomized, double-masked, controlled trial. *JAMA Neurol* **2013**, *70* (8),
37 981-7.
- 38 50. Sereda, M. W.; Meyer zu Horste, G.; Suter, U.; Uzma, N.; Nave, K. A.,
39 Therapeutic administration of progesterone antagonist in a model of Charcot-Marie-
40 Tooth disease (CMT-1A). *Nat Med* **2003**, *9* (12), 1533-7.
- 41 51. Pareyson, D.; Marchesi, C., Diagnosis, natural history, and management of
42 Charcot-Marie-Tooth disease. *Lancet Neurol* **2009**, *8* (7), 654-67.
- 43 52. Sahenk, Z.; Yalvac, M. E.; Amornvit, J.; Arnold, W. D.; Chen, L.; Shontz, K. M.;
44 Lewis, S., Efficacy of exogenous pyruvate in Trembler(J) mouse model of Charcot-
45 Marie-Tooth neuropathy. *Brain Behav* **2018**, *8* (10), e01118.
- 46 53. Pareyson, D.; Schenone, A.; Fabrizi, G. M.; Santoro, L.; Padua, L.; Quattrone, A.;
47 Vita, G.; Gemignani, F.; Visioli, F.; Solari, A.; Group, C.-T., A multicenter, randomized,
48
49
50
51
52
53
54
55

- 1
2
3 double-blind, placebo-controlled trial of long-term ascorbic acid treatment in Charcot-
4 Marie-Tooth disease type 1A (CMT-TRIAAL): the study protocol [EudraCT no.: 2006-
5 000032-27]. *Pharmacol Res* **2006**, *54* (6), 436-41.
- 6 54. Chumakov, I.; Milet, A.; Cholet, N.; Primas, G.; Boucard, A.; Pereira, Y.;
7 Graudens, E.; Mandel, J.; Laffaire, J.; Foucquier, J.; Glibert, F.; Bertrand, V.; Nave, K.
8 A.; Sereda, M. W.; Vial, E.; Guedj, M.; Hajj, R.; Nabirotkin, S.; Cohen, D., Polytherapy
9 with a combination of three repurposed drugs (PXT3003) down-regulates Pmp22 over-
10 expression and improves myelination, axonal and functional parameters in models of
11 CMT1A neuropathy. *Orphanet J Rare Dis* **2014**, *9*, 201.
- 12 55. Zhao, H. T.; Damle, S.; Ikeda-Lee, K.; Kuntz, S.; Li, J.; Mohan, A.; Kim, A.; Hung,
13 G.; Scheideler, M. A.; Scherer, S. S.; Svaren, J.; Swayze, E. E.; Kordasiewicz, H. B.,
14 PMP22 antisense oligonucleotides reverse Charcot-Marie-Tooth disease type 1A
15 features in rodent models. *J Clin Invest* **2018**, *128* (1), 359-368.
- 16 56. Ko, C. P.; Robitaille, R., Perisynaptic Schwann Cells at the Neuromuscular
17 Synapse: Adaptable, Multitasking Glial Cells. *Cold Spring Harb Perspect Biol* **2015**, *7*
18 (10), a020503.
- 19 57. Livak, K. J.; Schmittgen, T. D., Analysis of relative gene expression data using
20 real-time quantitative PCR and the 2(-Delta Delta C(T)) Method. *Methods* **2001**, *25* (4),
21 402-8.
- 22 58. Pareek, S.; Notterpek, L.; Snipes, G. J.; Naef, R.; Sossin, W.; Laliberte, J.;
23 lacampo, S.; Suter, U.; Shooter, E. M.; Murphy, R. A., Neurons promote the
24 translocation of peripheral myelin protein 22 into myelin. *J Neurosci* **1997**, *17* (20),
25 7754-62.
- 26 59. Amici, S. A.; Dunn, W. A., Jr.; Murphy, A. J.; Adams, N. C.; Gale, N. W.;
27 Valenzuela, D. M.; Yancopoulos, G. D.; Notterpek, L., Peripheral myelin protein 22 is in
28 complex with alpha6beta4 integrin, and its absence alters the Schwann cell basal
29 lamina. *J Neurosci* **2006**, *26* (4), 1179-89.
- 30 60. Gillespie, M. J.; Stein, R. B., The relationship between axon diameter, myelin
31 thickness and conduction velocity during atrophy of mammalian peripheral nerves. *Brain*
32 *Res* **1983**, *259* (1), 41-56.
33
34
35
36
37
38
39
40
41
42
43
44
45
46
47
48
49
50
51
52
53
54
55
56
57
58
59
60

For Table of Contents Only:

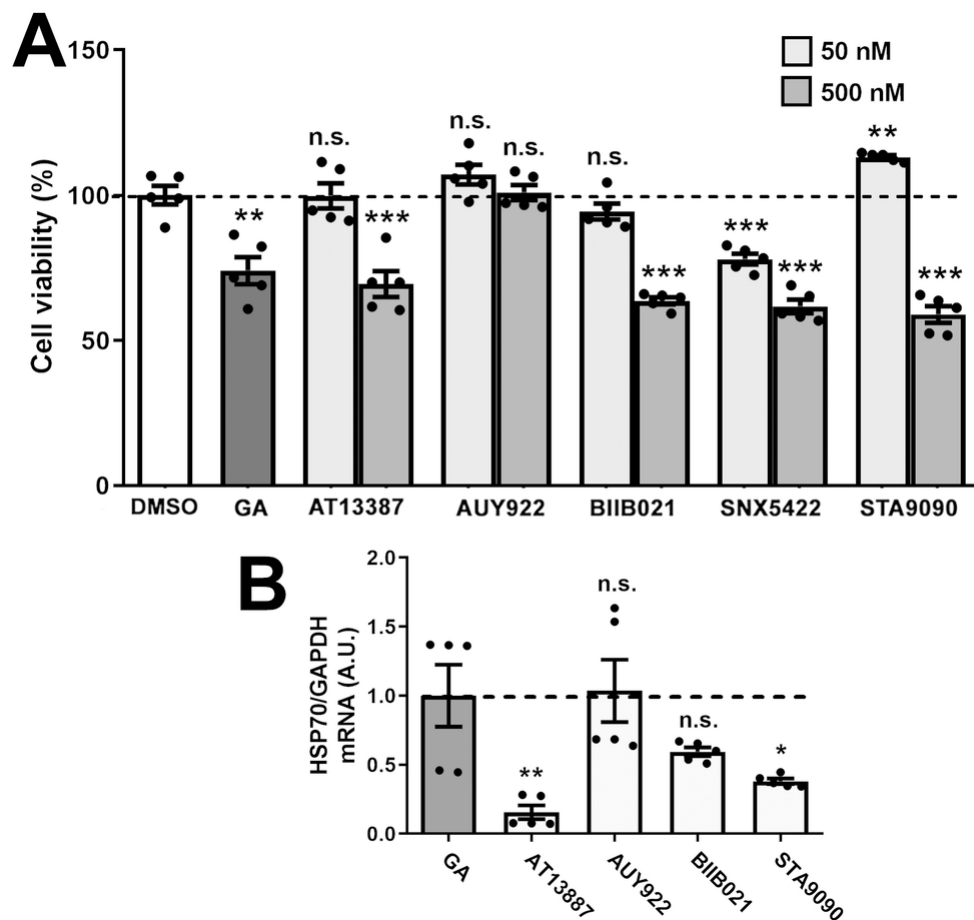


Figure 1. Effects of HSP90 inhibitors on Schwann cells. (A) Cell viability after treatment (24 h) with DMSO, GA (50 nM) or the indicated five HSP90 inhibitors (50 and 500 nM) was calculated and graphed, as percentage of DMSO (vehicle). (B) HSP70 mRNA levels were quantified after 24 h treatment with the indicated compounds (100 nM). GAPDH was used as an internal control. (A, B) GA (50 nM) served as a positive control. A.U.: arbitrary units. Graphs are plotted as means + SEM; *** $P < 0.001$; ** $P < 0.01$; * $P < 0.05$; n.s. non-significant; two-tailed Unpaired Student's t-test.

84x78mm (300 x 300 DPI)

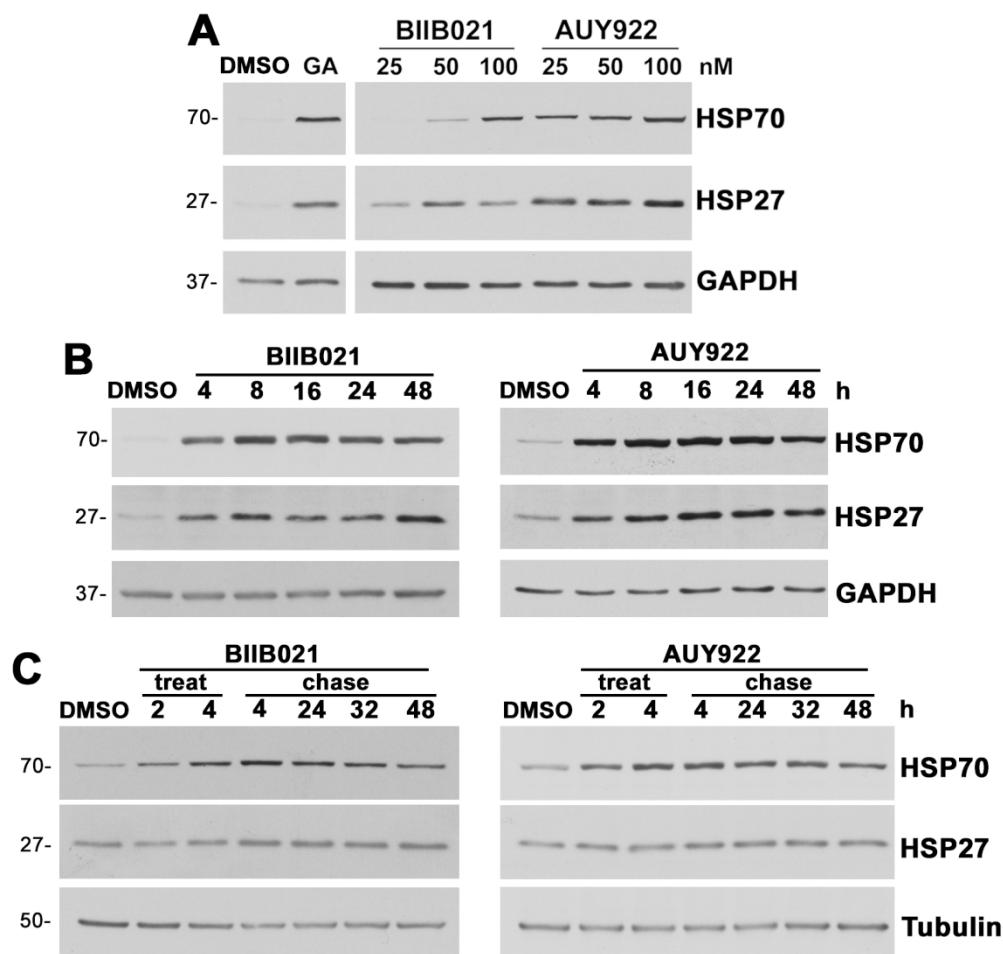


Figure 2. Treatment with BIIB021 and AUY922 increase chaperone expression in a dose- and time-dependent manner. (A) Steady-state levels of HSP70 and HSP27 in whole Schwann cell lysates (15 μ g/lane) were analyzed after 24 h treatment with DMSO, BIIB021 or AUY922, at the specified doses. GA (50 nM) served as a positive control. (B) HSP70 and HSP27 levels were observed after treatment with 100 nM BIIB021 or AUY922 for the indicated times. (C) Chaperone pathway activation by BIIB021 or AUY922 (100 nM) was studied after 2 or 4 h (treatment), followed by 4, 24, 32 and 48 h chase time points. (A, B) GAPDH and (C) tubulin served as protein loading controls. Molecular mass on left, in kDa. (A-C) Data shown are representative of n=3 independent experiments.

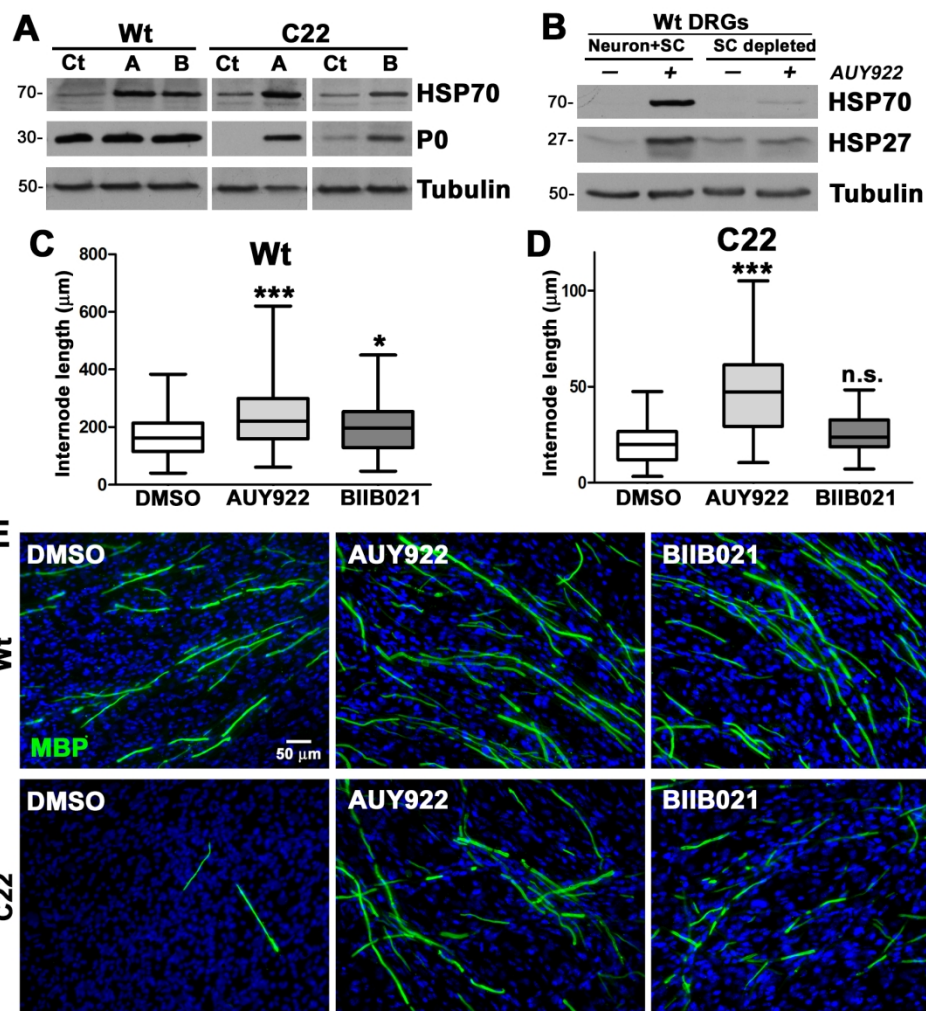


Figure 3. Improved myelin production in DRG explant cultures from C22 mice after treatment with AUY922. (A) Steady-state levels of HSP70 and P0 were analyzed in Vehicle (Veh), AUY922 or BIIB021 treated explant lysates (35 μg/lane). (B) Wt DRG cultures, with (Neuron + Schwann cell), and without (depleted), Schwann cells were treated with 100 nM AUY922 and analyzed for the indicated chaperones. (A, B) Tubulin served as a protein loading control. Molecular mass on left, in kDa. (C, D) MBP-positive myelin internode lengths in explant cultures from Wt (C) and C22 (D) mice treated with Vehicle, AUY922 or BIIB021 were measured (n=100-120 segments per group) and graphed as whisker plots with median (center line), quartiles (box), and extremes (whiskers); ***P<0.001; *P<0.05; n.s. non-significant; two-tailed Unpaired Student's t-test. (E) Cultures from Wt (top panel) and C22 (lower panel) mice, treated with the indicated compounds were stained for MBP (green). Nuclei were visualized with Hoechst dye (blue). Scale bar, as shown. Data shown are representative of n=3-4 independent experiments.

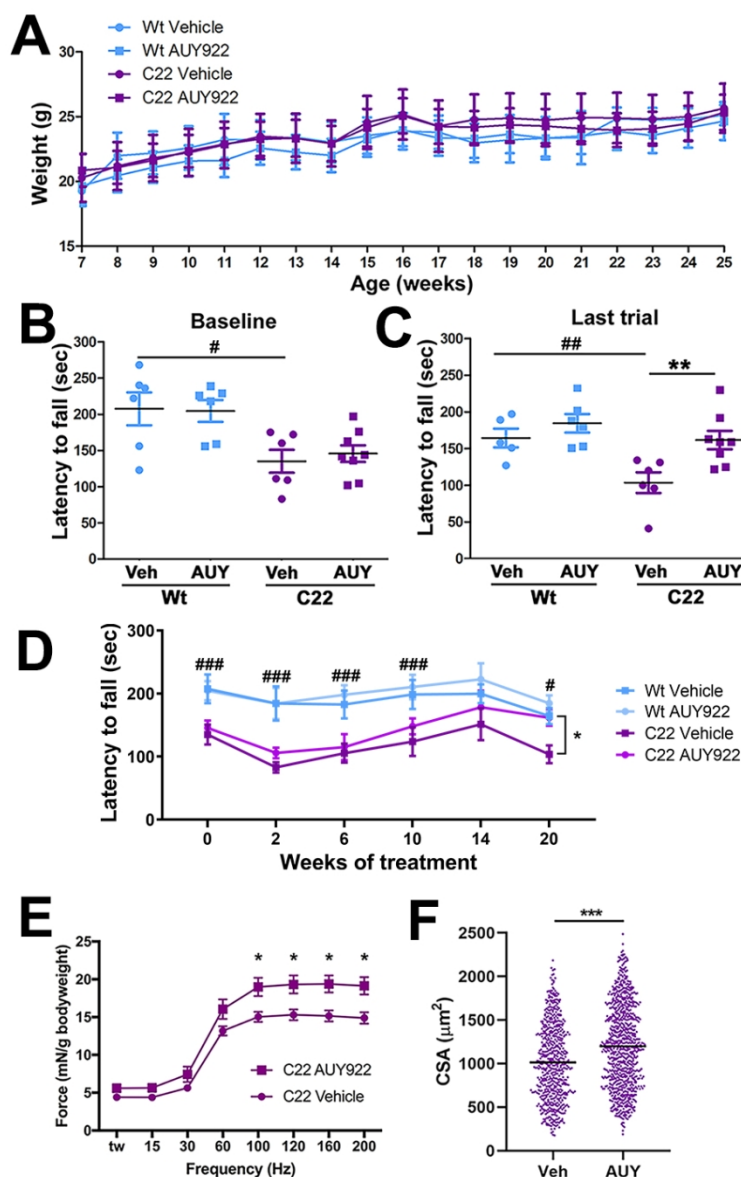


Figure 4. Treatment with AUY922 improves neuromuscular performance of C22 mice. (A) Mean + SEM of body weight of Wt and C22 mice ($n=6-8$ mice per group) were plotted over the treatment period. (B-C) Performance of individual animals on the accelerating rotarod at (B) baseline (7 weeks age) and (C) at the end of the treatment (25 weeks age) are shown. The bars represent the mean for each group. (D) Mean + SEM of rotarod performance of all groups, plotted over the treatment period. (E) Muscle force, analyzed using an in situ technique, was recorded and normalized to the animal's body weight (mN/g = milliNewtons/grams). Each point represents the mean + SEM force. (F) Distribution of individual measures of cross-sectional area of TA muscle from C22 mice treated with vehicle or AUY ($n=3-5$ mice per group). The bars represent the mean for each group. For all graphs, # signs indicate a significant ($\#P<0.05$, $\#\#P<0.01$, $\#\#\#P<0.001$) genotype difference. $*P<0.05$, $**P<0.01$, $***P<0.001$, indicating a significant treatment effect for C22 mice.

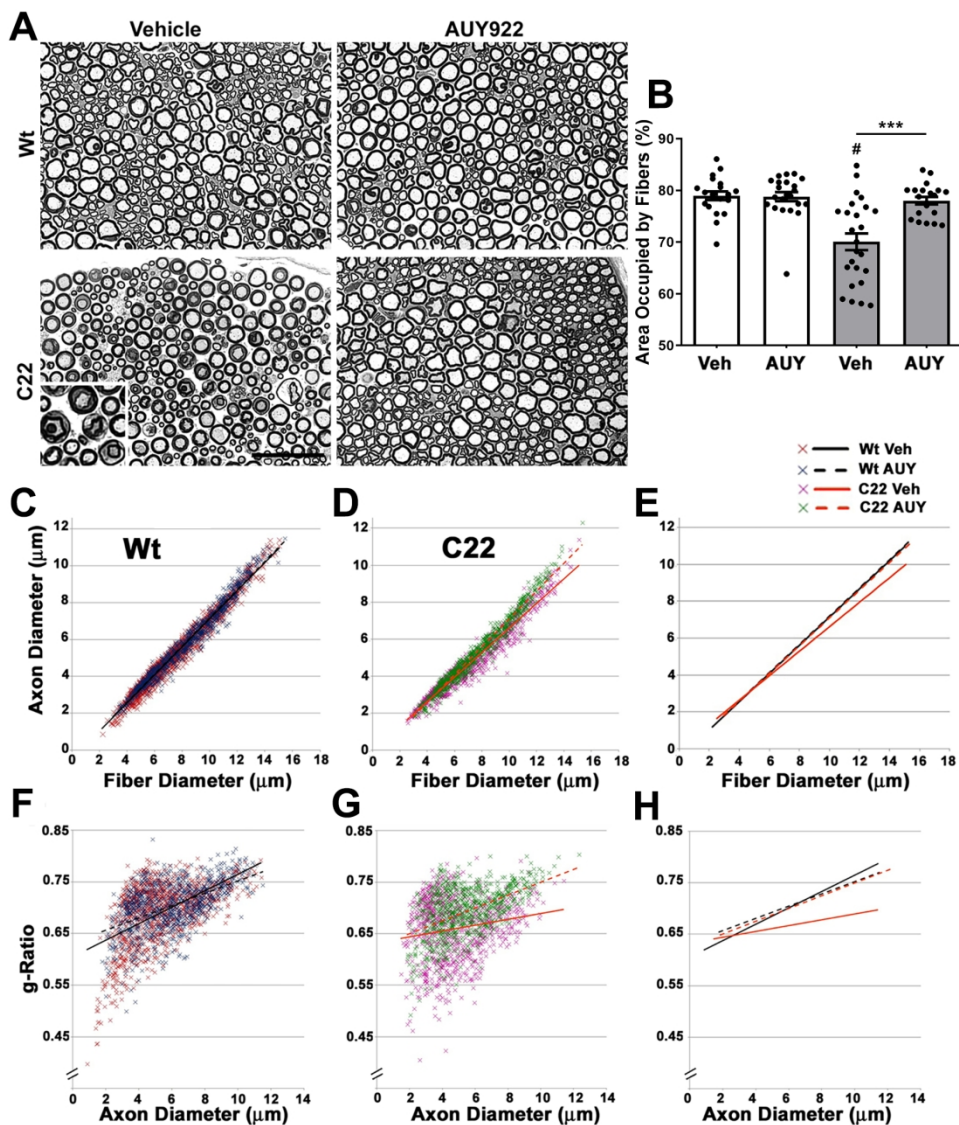


Figure 5. AUY922 administration supports the maintenance of myelinated axons in sciatic nerves of C22 mice. (A) Cross-sectional views of nerve sections from Wt (top panels) and C22 (lower panels) male mice. Micron bar, 45 μm . (B) Cross-sectional area occupied by nerve fibers in a 40 μm X 40 μm square (n=20-25 fibers per animal; n=6-8 mice per group) was measured and graphed as shown. Graph plotted as means + SEM; ***P<0.001, across the treatment groups; #P<0.05, across the genotypes; two-tailed Unpaired Student's t-test. (C-D) Correlative analyses between axon and fiber diameter measurements were obtained from sciatic nerve cross-sectional areas from (C) Wt and (D) C22 groups. (E) Comparison of trendlines between the cohorts in C and D. (F-G) Scatter plots comparing the g-ratios (axon diameter/fiber diameter) of individual fibers plotted as a function of axon diameters in nerves of (F) Wt and (G) C22 animals. (C-H) n=950-1100 fibers per group. (H) Trendline comparisons of graphs in F and G.

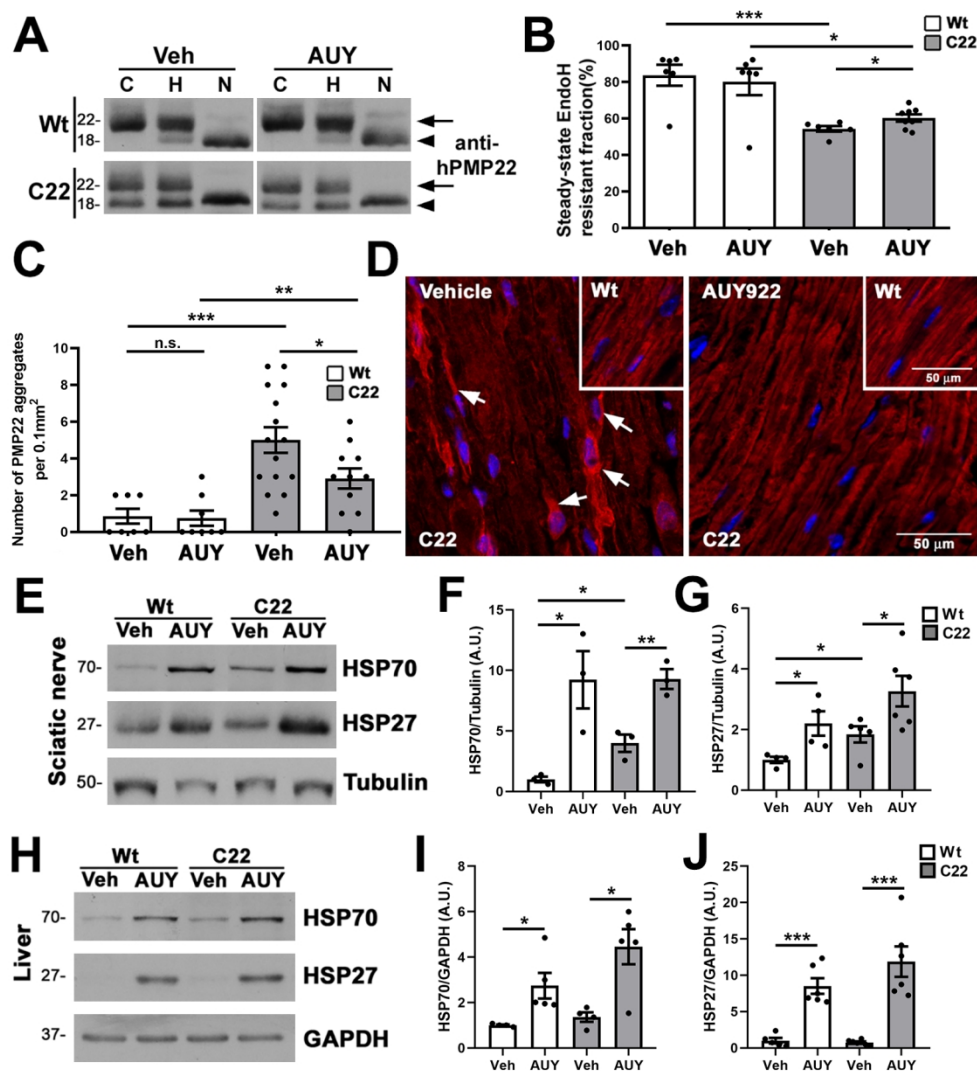


Figure 6. Improved processing of PMP22 in AUY922 treated C22 mice. (A) Sciatic nerve lysates (5 μ g/lane) were treated with either EndoH (H) or PNGaseF (N) and probed with anti-human PMP22 antibodies. No enzyme samples served as controls (C). EndoH-resistant (arrows), and EndoH-sensitive (arrowheads) PMP22 fractions are marked. (B) Quantification of EndoH-resistant PMP22 fractions in sciatic nerves. (C) PMP22-positive aggregates per microscopic field (0.1 mm²) were counted in longitudinal sections of sciatic nerves. (D) Representative images of anti-PMP22 antibody stained (red) nerve sections from Wt (insets) and C22 mice are shown. Arrows mark PMP22-positive aggregates. Hoechst dye (blue) was used to visualize the nuclei. Scale bars, as shown. (E) Steady-state levels of HSP70 and HSP27 in vehicle (Veh) and AUY922 (AUY) treated nerve lysates (30 μ g/lane) were (F, G) quantified from independent western blots. (H) Whole liver lysates (30 μ g/lane) were processed for (I, J) HSP70 and HSP27 quantification. (E-J) GAPDH or Tubulin served as a loading control. Molecular mass on left in kDa. (B, C, F, G, I, J) n=3-8 mice per group and plotted as means + SEM; ***P<0.001; **P<0.01; *P<0.05; n.s. non-significant; two-tailed Unpaired Student's t-test.

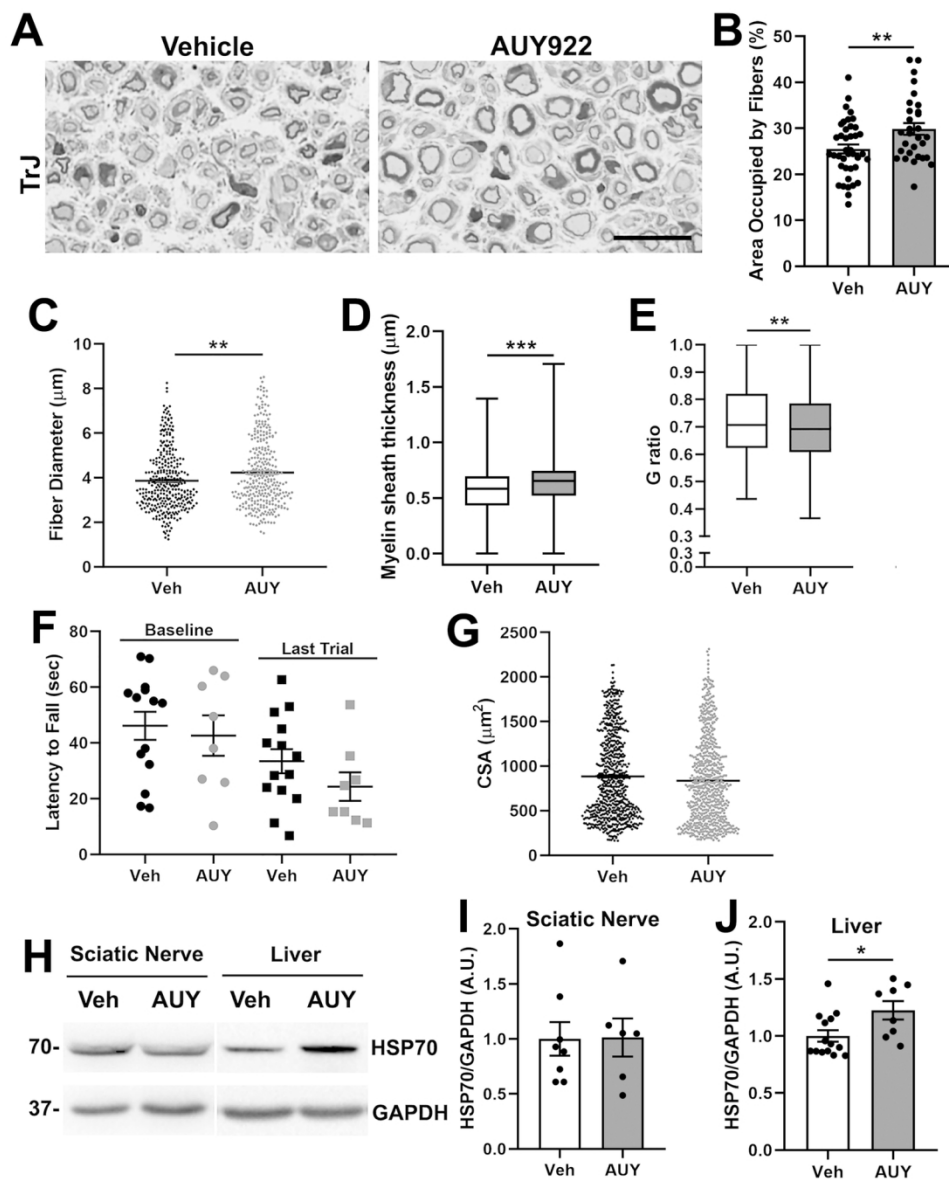


Figure 7. AUY922 promotes the maintenance of myelinated axons in TrJ mice. (A) Cross-sectional views of nerve sections from vehicle- (left) and AUY-treated (right) TrJ mice. Micron bar, 20 μm . (B-E) Morphometric analysis of nerves from vehicle and AUY-treated TrJ mice ($n=4$ mice, 320 fibers, 30-40 areas per group). (B) Percent area occupied by fibers, (C) fiber diameter, (D) myelin sheath thickness, and (E) G ratios were graphed. (F) Rotarod performance at baseline and at the end of treatment is shown for vehicle or AUY-treated TrJ mice. (G) Myofiber cross-sectional area of TA muscle from the indicated groups ($n=5$ mice, 695 fibers per group). (H) Sciatic nerve (30 $\mu\text{g}/\text{lane}$) and whole liver lysates (30 $\mu\text{g}/\text{lane}$), with (I, J) quantification, from vehicle (Veh) and AUY922 (AUY) treated TrJ mice, were assessed for HSP70. (H-J) $n=6-14$ mice per group, with GAPDH serving as a loading control. Molecular mass on left, in kDa. Graphs plotted as means (C, G) + SEM (B, F, I, J), or as whisker plots with median (center line), quartiles (box), and extremes (whiskers) (D, E); **** $P<0.001$; ** $P<0.01$; * $P<0.05$; two-tailed Unpaired Student's t-test.

135x167mm (300 x 300 DPI)

1
2
3
4
5
6
7
8
9
10
11
12
13
14
15
16
17
18
19
20
21
22
23
24
25
26
27
28
29
30
31
32
33
34
35
36
37
38
39
40
41
42
43
44
45
46
47
48
49
50
51
52
53
54
55
56
57
58
59
60